Hochschule Neubrandenburg
Fachbereich LGGB
Studiengang Geoinformatik und Geodäsie

Retrieval of plasmaspheric Total Electron Content from space-based GPS observations including a receiver differential code bias and multipath estimation

Masterthesis

vorgelegt von: Max Noja
geboren am: 17.08.1983

Zum Erlangen des akademischen Grades

Master of Engineering (M.Eng.)

Abstract

The ionosphere and plasmasphere denote the ionized parts of the upper atmosphere. The electron and ion density and their gradients have a significant influence on the propagation of trans-ionospheric radio waves as used by satellite-based navigation systems like GPS, GLONASS, or the future Galileo system, affecting the navigational solution for positioning. Therefore, it is of great interest to determine and correct the ionospheric path delay. In doing so, Total Electron Content (TEC), the integrated number of free electrons along the radio wave path, is an essential measurement to develop empirical and physical models of the near-Earth space.

This master thesis describes a procedure to retrieve TEC on the basis of GPS observations. This procedure provides a near real-time calculation of TEC values including a receiver differential code bias and a multipath estimation. The development of the procedure is based on measurements from the navigation antenna of the multi-year satellite mission CHAMP, which offers GPS observations from almost ten years.

Kurzfassung

Die Ionosphäre und Plasmaphäre bilden den ionisierten Anteil der oberen Atmosphäre. Die Elektronen- und Ionendichte sowie deren Gradienten wirken sich in großem Maße auf die Laufzeit von trans-ionsphärischen Radiowellen aus und beeinträchtigen dadurch z.B. die Positionsbestimmung mit satellitengestützten Navigationssytemen wie GPS, GLONASS oder dem zukünftigen Galileo-System. Deshalb besteht ein großes Interesse, die ionosphärische Laufzeitverzögerung zu bestimmen und zu korrigieren. Dabei ist der Gesamtelektronengehalt, engl.: Total Electron Content (TEC), eine entscheidende Messgröße zur Erstellung von empirischen und physikalischen Modellen des erdnahen Weltraums.

Diese Arbeit beschreibt einen Verfahren zur Bestimmmung des TEC auf Grundlage von GPS-Beobachtungen. Das Verfahren ermöglicht eine zeitnahe Berechnung des TEC inklusive einer Schätzung des Mehrwegeeffekts sowie des instrumentellen Laufzeitfehlers des GPS-Empfängers. Die zur Entwicklung des Verfahrens verwendeten Daten stammen von der Navigationsantenne der langjährigen Satellitenmission CHAMP, welche GPS-Messungen von annähernd zehn Jahren bereithält.

Contents

1. Introduction and objectives

The sun's radiation causes an ionization in the upper regions of the Earth's atmosphere, which is then called the *ionosphere.* This ionization is an important concern in the operation of trans-ionospheric radio communication since it effects the propagation of radio waves. This especially holds for the signals of satellite-based navigation systems such as GPS or GLONASS, which make use of high frequency radio waves. When passing through the ionosphere, the signals of these systems interact with the ionized air, which is able to strongly degrade the navigational solution. The influence of the ionosphere on radio waves is proportional to the electron density and inversely quadratically proportional to the frequency of the radio waves. After a proper calibration, these properties of the signals can be used to determine the integrated electron content along the path of the radio waves, which is called *Total Electron Content* (TEC). TEC denotes an essential source of information to space weather applications. GPS TEC is the basic input to data assimilation models, imaging and now- and forecasting the ionosphere (Scherliess et al. (2009), Bust and Mitchell (2008)). These models are necessary to correct the signals of satellite-based navigation systems in order to enable a proper positioning. Ionospheric remote sensing to determine TEC is mainly realized by ground-based GPS receivers covering populated areas. A wide GPS tracking network is maintained by the International GNSS Service (IGS) with ground-stations distributed over all continents. However, certain areas such as the oceans or polar regions are not well covered. An ideal complement are GPS observations from Low Earth Orbit (LEO) satellites, allowing for an ionospheric remote sensing with global coverage. Using GPS observations of satellite navigation antennas, which are mostly adjusted upwards, additionally enables a precise remote sensing of the topside ionosphere, which is generally obscured in ground-based GPS observations by the much higher ionized lower ionospheric regions.

The main objective of this work is to develop a retrieval method for topside ionospheric and plasmaspheric Total Electron Content from space-based GPS observations. The most important properties of this method are the estimation of multipath errors and instrumental biases of the GPS observations, as well as a near real-time calculation of TEC in the range of seconds. The development of this retrieval method is based on data from the multi-year LEO satellite mission CHAMP, which offers GPS observations from approximately ten years. As the CHAMP mission will come to an end in the near future, the results of this work are mainly intended to be applied to the upcoming ESA satellite mission Swarm, which consists of three satellites similar to the CHAMP satellite.

2. Background

This section provides the scientific background of this work. It includes an introduction to the ionosphere and Total Electron Content, an explanation of the atmospheric impact on the propagation of electromagnetic waves, an overview of NAVSTAR-GPS, and a description of the CHAMP satellite mission.

2.1. The Ionosphere

The ionosphere denotes the ionized part of the Earth's upper atmosphere. This layer of the atmosphere emerges from solar radiation. Due to low air density, solar radiation leads to a continuous ionization in regions above approximately 80 km height. Thereby released free carriers of charge are mainly electrons and singly charged ions which appear in an even distribution so that the ionospheric plasma is neutral to the outside. The ionosphere is characterized by the electron density, which also represents the level of ionization. The ionization degree is less than one percent and depends mostly on solar activity, air density, and air composition. The Earth's magnetic field has a considerable impact on the ionosphere. It guides the free carriers of charge, causing the formation of electric currents and electric fields in the ionosphere.

The ionosphere has a layered structure with a strong vertical gradient which is due to the height dependent density and composition of the air. An illustration of the ionosphere's structure with the typical electron density and the predominant ionized atoms and molecules is given in Fig. 1. The lowest layer is referred to as the *D region* with the least ionization and emerges in a height between 80 and 90 km and only during daytime due to a high rate of electron-ion recombination after sunset. The D region is followed by the *E region* in a height between 90 and 130 km. This layer also exists only during daytime. The subsequent layer is the *F region* from approximately 200 to 1000 km. During daytime the F region is separated into the F1 region and the F2 region. The F1 region reaches from $\approx$ 130 to 200 km and also emerges only during daytime due to the loss of ionization after sunset. The F2 region ranges from $\approx$ 200 to 400 km and has the highest level of ionization. Due to the high electron density and a low rate of electron-ion recombination, the F2 region also exits at night. Above the region with the peak electron density, the topside ionosphere begins, which is a transitional layer to the upmost region of the ionosphere, the *plasmasphere*, which is also referred to as protonosphere. The beginning of the plasmasphere is characterized by the transition of predominantly present O^+ ions to H^+ ions, which can vary between 600 and 2000 km (Prölss, 2004). The plasmasphere ends with the *plasmapause* as its boundary.
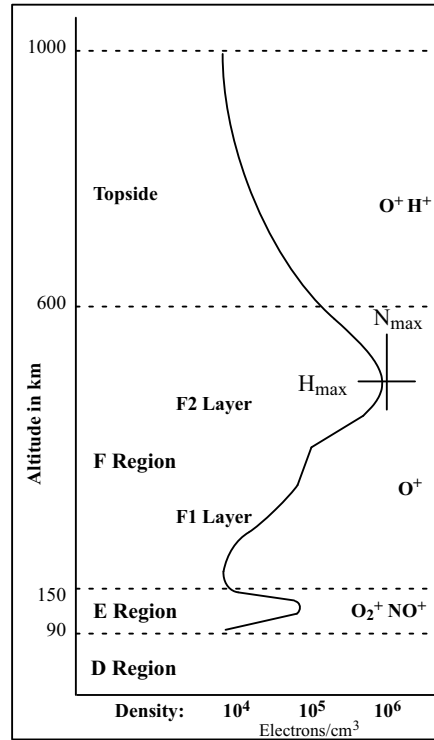
Figure 1: Structure of the ionosphere (image source: Anderson and Fuller-Rowell (1999))

2.1.1. Total Electron Content

Besides the electron density, Total Electron Content (TEC) denotes another important quantity for describing the ionosphere. Ionospheric TEC is the integral over the electron density distribution N_e along a distinct path s. During the course of this work, TEC always refers to the integrated electron density along a slant path which is also called sTEC (slant TEC) with:

$$TEC \equiv sTEC = \int N_e(s)ds \qquad (1)$$

The unit of TEC is TEC Unit (TECU) with 1 TECU = 10^{16} electrons per m^2.

2.2. Atmospheric impact on the propagation of electromagnetic waves

Electromagnetic waves passing through the atmosphere experience a change of phase, amplitude, polarization, and speed. This interaction can be used to derive ionospheric information from electromagnetic waves such as TEC.

2.2.1. Atmospheric refractive index

The refractive index n of a medium is generally described by:

$$n = \frac{c}{v} \tag{2}$$

where c denotes the speed of light in vacuum and v the speed of the wave in the medium. The atmospheric refractive index can be divided into a tropospheric and an ionospheric part. The tropospheric refractive index is mainly characterized by the neutral gases in the atmosphere. The density of the neutral gases decreases with increasing height. In heights above approximately 60 km the tropospheric refraction is negligible due to low air density. In the ionospheric regions of the atmosphere the propagation of electromagnetic waves is mainly influenced by the presence of free electrons. The ionosphere is furthermore a dispersive propagation medium with a complex refractive index. However, for radio waves with a frequency above 100 Mhz as used by GPS, the ionospheric refractive index can be assumed to be real (Heise, 2002). In the first approximation and by neglecting the terms of third order and fourth order, the ionospheric refractive index n_{ion} is described by:

$$n_{ion} = 1 - \frac{K}{f^2} N_e \tag{3}$$

When describing the ionospheric impact on a signal modulated onto a radio wave, the ionospheric group index n_{Gion} has to be used instead (see Hartmann and Leitinger (1984)) which is decribed by:

$$n_{Gion} = 1 + \frac{K}{f^2} N_e \tag{4}$$

In both equations K denotes a constant with the value of 40.3 $m^3 s^{-2}$, and f denotes the frequency of the radio wave. Equations (3) and (4) denote the common approximations of the ionospheric refractive index which are used for the determination of TEC from GPS observations.

2.2.2. Optical path length

The propagation of electromagnetic waves through a non-vacuum medium such as the atmosphere can be described by Fermat's principle:

$$\int_T^R n(s)ds = min. \tag{5}$$

Fermat's principle says that a wave passing through a medium with a space- and time-varying refractive index follows the shortest possible way from transmitter T to receiver R. The refractive index along the ray path s is denoted by $n(s)$. The optical path length L of the ray path between receiver and transmitter is described by:

$$L = \int_T^R n(s)ds \tag{6}$$

The ray path between receiver and transmitter deviates from the straight-lined geometrical path when the refractive index is different from 1. To clarify this, equation (6) can be rewritten as:

$$L = \int_T^R (n(s)-1)ds + \int_T^R ds = \int_T^R (n(s)-1)ds + \rho + \Delta\rho \tag{7}$$

Here, ρ denotes the straight-lined geometrical distance and $\Delta\rho$ denotes the deviation from the straight ray path. For electromagnetic waves passing through the troposphere and the ionosphere the optical path length is given by:

$$L = \rho + \Delta_{trop} + \Delta_{ion} \tag{8}$$

with

$$\Delta_{trop} = \Delta\rho_{trop} + \int_T^R (n_{trop}-1)ds \ \text{ and } \ \Delta_{ion} = \Delta\rho_{ion} + \int_T^R (n_{ion}-1)ds$$

where Δ_{trop} is called the tropospheric propagation error and Δ_{ion} the ionospheric propagation error. For high frequency radio waves such as the GPS signals, the geometric part $\Delta\rho_{ion}$ of the ionospheric propagation error is very small and can be neglected so that a nearly straight propagation of the radio waves can be assumed (Heise, 2002). Considering the ionospheric refractive indices from equations (3) and (4) and equation (1) for TEC, the ionospheric propagation error can be approximated by:

$$\Delta_{ion} = \pm\frac{K}{f^2}TEC \tag{9}$$

This approximation forms the basis for the retrieval of ionospheric TEC from GPS observations.

2.3. NAVSTAR - GPS

The *Navigation System for Timing and Ranging* (NAVSTAR) or more commonly known as *Global Satellite System* (GPS) is a Global Navigation Satellite System (GNSS) realized by the American Department of Defense (DoD) to provide a globally available system for the highly precise determination of position, velocity, and time, mainly intended for military purposes. GPS is based on a network of satellites continuously broadcasting coded messages. Using an appropriate receiver, the messages of the satellites can be received and decoded. To reserve high precision positioning for military purposes, the code information is provided with two different services: the *Precise Positioning Service (PPS)* for authorized users of the DoD and the *Standard Positioning Service (SPS)* for civil users.

The basic principle of GPS is the determination of the distance between receiver and transmitter. From the signals of at least four different GPS satellites both the three-dimensional position of the receiver and the respective change in time can be determined, resulting in the navigation solution of GPS. For a thorough explanation of GPS and its navigation principle the reader is referred to specialized literature (e.g. Bauer (2002), Seeber (2003)).

2.3.1. System segmentation

GPS consists of three major operational segments, the *space segment*, the *control segment*, and the *user segment.* The space segment is composed of the satellites and their constellation. GPS originally started with 24 satellites, but consists of 31 active satellites since March 2008, which provides a number of approximately eight satellites globally available at any time. The control segment is responsible for the proper operation of GPS. Its main tasks are the surveillance of the satellite orbits, the maintenance of the satellite health, the prediction of the satellite ephemerides, and the update of the satellite navigation message. Both the space and control segment are under the responsibility of the DoD.

The user segment comprises the military users of the PPS and the civil users of the SPS. The civil use of GPS includes the industrial development of GPS receivers for commercial purposes and their sale, for example in car navigation systems, as well as scientific applications, which mainly include applications in geodesy. GPS receivers are often characterized by their number of channels, which correspond to the number of satellites that can be monitored simultaneously. Modern GPS receivers offer 12 to 20 channels, which allows for a highly precise positioning with an adequate number of available satellites.

2.3.2. Navigation signals

To enable navigation and positioning, each GPS satellite continuously broadcasts two L-Band (1,000 - 2,000 Mhz) signals at 1.57542 GHz (L1 signal) and 1.2276 GHz (L2 signal), as well as a navigation message at 50 Hz containing the GPS week number, satellite health information, ephemerides, and an almanac. The determination of the distance between receiver and transmitter using only pure carrier waves is based on the phase shift between the transmitted and received signal. Since this carrier phase shift does not contain any information about the number of whole wave cycles of the ray path, the distance between receiver and satellite based on carrier phases is only relative and cannot be determined in real-time. To accomplish real-time navigation, the necessary information is modulated onto the carrier phases of L1 and L2 using pseudo-random-noise (PRN) codes, which are mathematically generated sequences of zeroes and ones. Each satellite transmits two PRN codes, the *Coarse/Aquisition code (C/A-code)* modulated on L1 and the *Precision code (P-code)* modulated on L1 and L2. A schematic illustration of the carrier phase modulation is given in Fig. 2.
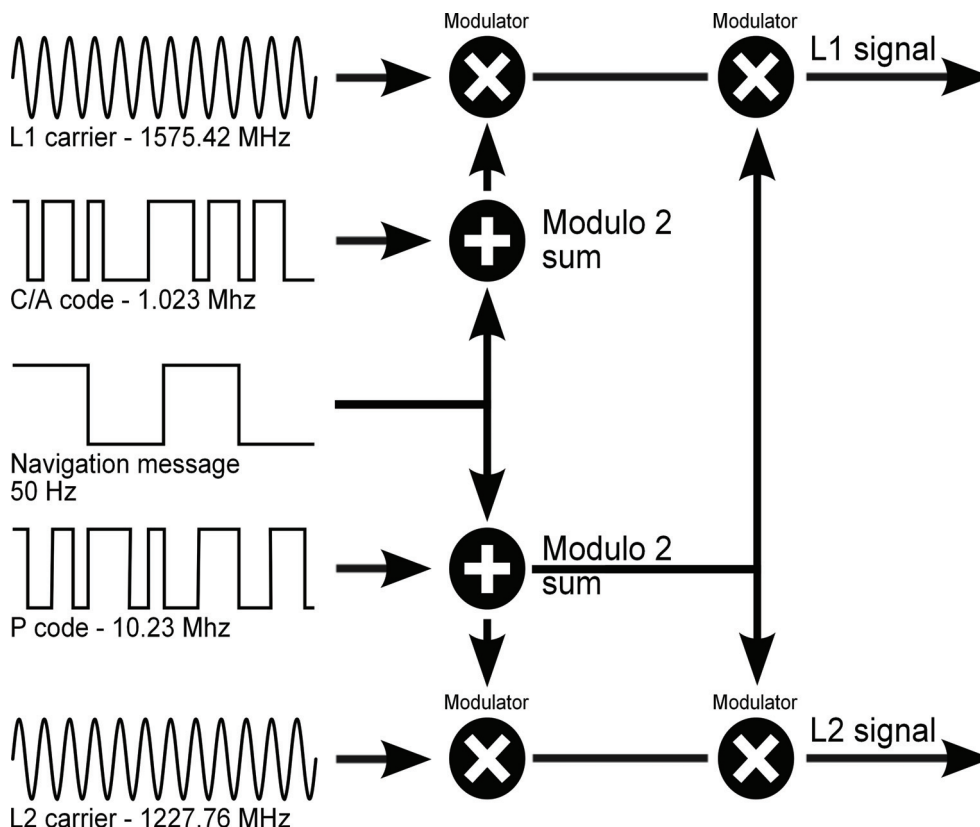
Figure 2: GPS carrier phase modulation (according to Dana (1998))

The C/A-code is publicly available and intended for civil usage. It has a length of 1,023 bits, so-called chips, transmitted at a frequency of 1.023 Mhz. These chips do not contain any information and are used only for signal reception. The PRN sequence of the C/A-code is unique for each GPS satellite and repeats itself every millisecond. Multiplying the carrier wavelength with the ratio of the carrier frequency to the chip rate results in the "length" of one chip with approximately 300 m. The inaccuracy of a single range measurement with C/A code is $c \cdot 0.001s \approx 300\ km$. To get a more precise range measurement, a higher chip rate is needed.

The chips of the P-code are generated at a higher rate with 10.23 million chips per second. The PRN sequence of the P-code is much longer with 266 days, providing a seven-day segment for each GPS satellite. As the segments do not overlap, each GPS satellite is also identified by its PRN sequence. However, an important limitation to the civil usage of the P-code is its encryption to the Y-code with the secret W-code. This encryption is called *Anti-Spoofing (AS)*. AS is applied to avoid spoofing of GPS receivers with adversary signals. AS has been permanently activated since January 31, 1994. Another limitation for P-code observations was the so-called *Selected Availability (SA)*, which was aimed at degrading the signal precision due to security concerns. SA has been deactivated since May 2, 2000. This results in a higher precision for the civil usage of GPS.

2.3.3. Observation equations

Using code phase observations to determine the distance between receiver and satellite results in so-called pseudo-ranges. Pseudo-ranges are propagation delay measurements which contain a number of errors including tropospheric and ionospheric propagation errors, satellite and receiver clock errors, instrumental biases of the receiver and satellite, as well as multipath and noise. Accounting for the additional errors, the observation equation for pseudo-ranges is defined by:

$$P_R^S = \rho_R^S + c(\Delta t_S - \Delta t_R) + \Delta_{trop} + \Delta_{ion} + c(b_S + b_R)_P + \varepsilon_P \tag{10}$$

with

P_R^S pseudo-range between receiver and transmitter expressed in length units,

ρ_R^S geometrical distance between receiver and transmitter,

c speed of light,

Δt_S satellite clock error,

Δt_R receiver clock error,

Δ_{trop} tropospheric propagation error,

Δ_{ion} ionospheric propagation error,

b_S instrumental bias of the satellite,

b_R instrumental bias of the receiver, and

ε_P multipath and noise.

Using carrier phase observations instead of code phase observations, the observation equation becomes:

$$L_R^S \equiv \phi\lambda = \rho_R^S + c(\Delta t_S - \Delta t_R) + \Delta_{Trop} - \Delta_{Ion} + N\lambda + c(b_S + b_R)_L + \varepsilon_L \qquad (11)$$

with

L_R^S carrier range expressed in length units,

ϕ number of wave cycles,

N carrier phase ambiguity, and

λ carrier wave length.

The main difference in comparison to the code phase observation equation is the opposite sign of the ionospheric propagation error and the unknown number of whole wave cycles N (carrier phase ambiguity) along the ray path, which make the carrier range only a relative distance. For reasons of clarity, the subscripts of L1, L2, P1, and P2 have been omitted in equations (10) and (11).

Both observation equations contain frequency dependent and frequency independent terms. By subtracting code phase and carrier phase observations on both frequencies, all frequency independent terms are omitted, leaving only the ionospheric propagation error and the measurement dependent carrier phase ambiguities, instrumental biases, and noise. After an appropriate calibration of the measurement dependent terms, TEC along a ray path can be derived from the ionospheric propagation error. A detailed description of the TEC determination from GPS observations is given in section 3.1.

2.4. The CHAMP mission

CHAMP (CHAllenging Minisatellite Payload) is a German satellite mission with various objectives in scientific research and application. The CHAMP satellite was launched on July 15, 2000 from the cosmodrome Plesetsk, Russia with an initial altitude of 454 km, which makes CHAMP a LEO mission. The CHAMP satellite is on a near polar orbit with an inclination of 87.3°, orbiting the Earth almost circularly. The CHAMP mission was initially designated for a life time of five years, but is still running as of July 2010. CHAMP is under the direction of the German Research Centre for Geosciences GFZ, Potsdam in cooperation with the German Aerospace Center DLR, as well as several aerospace industry companies such as EADS Astrium and Daimler-Chrysler Aerospace who constructed the satellite.

2.4.1. Science objectives

The CHAMP mission has three main scientific research objectives:

- Analysis and research of the Earth's gravitational field including its temporal and spatial variation.

- Determination and observation of the Earth's magnetic field on the ground and in near-Earth space.

- Limb sounding of the Earth's atmosphere and ionosphere using GPS radio occultation measurements.

2.4.2. Satellite system

To accomplish the mission objectives, there is a number of scientific instruments aboard CHAMP to carry out necessary measurements. An illustration of the front and the rear side of the CHAMP satellite and its instrumentation is given in Fig. 3. At the front side, CHAMP has a boom of 4 metres length where an Overhauser magnetometer and a Fluxgate magnetometer with star sensors are situated. The Overhauser magnetometer is used for a precise scalar measurement of the magnetic field, and the Fluxgate magnetometer is used to determine the vectorial components of the magnetic field. The star sensors are required to determine CHAMP's attitude. The Earth's magnetic field is further investigated with a digital ion drift meter in conjunction with a Langmuir probe situated at the bottom side of the satellite. These instruments are used to measure electron density and temperature.
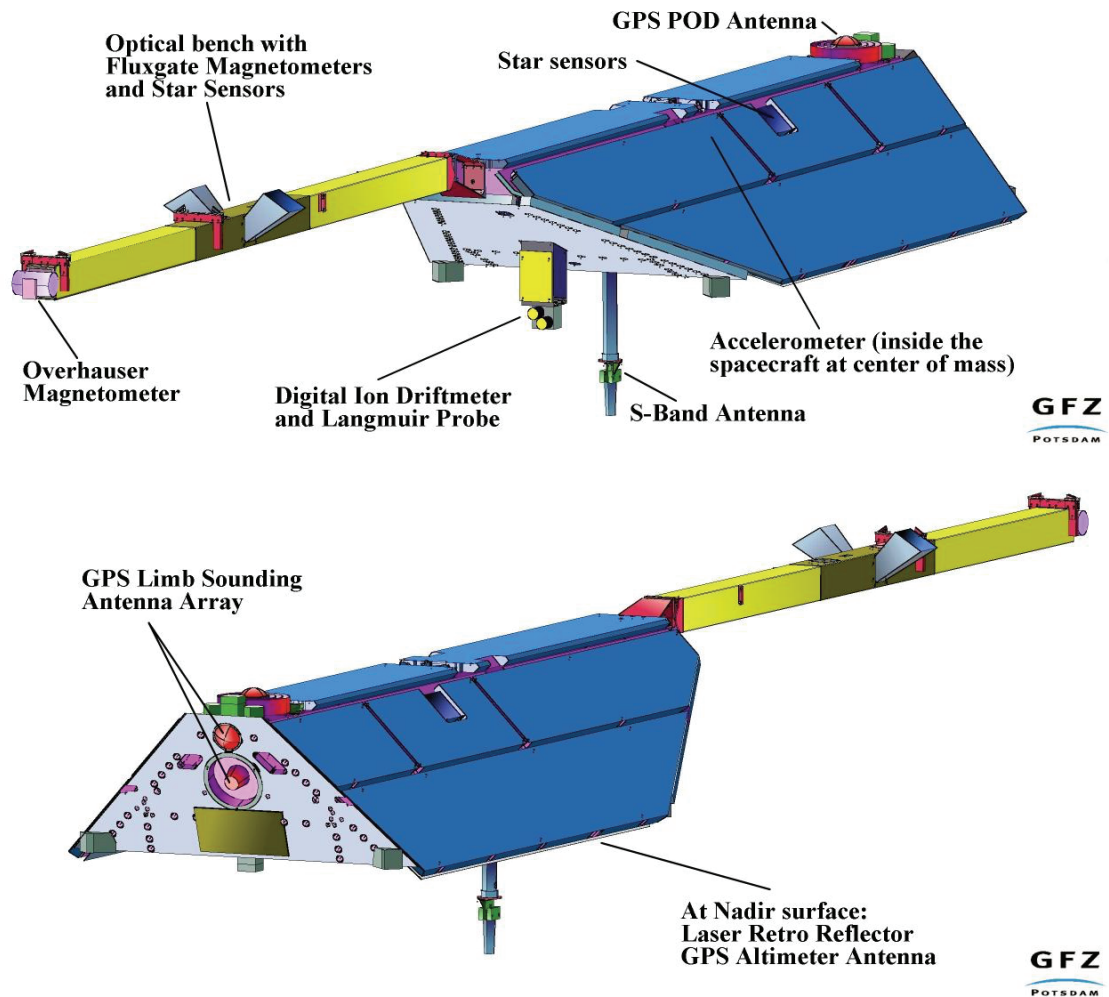
Figure 3: CHAMP satellite with instrumentation (image source: CHAMP website (Lühr, 2010))

Furthermore, there is a laser retro reflector located at the bottom side of the satellite to determine the distance between ground stations and the satellite. For a precise orbit determination CHAMP employs a TRSR-2 GPS receiver. Besides determining CHAMP's orbit position, the GPS receiver in conjunction with its four antennas is also used for gravitational field recovery, occultation measurements of the atmosphere and ionosphere, and GPS altimetry. Additionally, CHAMP has an electrostatic STAR accelerometer at the center of the satellite's mass for measuring non-gravitational accelerations. This accelerometer also contributes to orbit determination. Since the GPS measurements of the CHAMP POD antenna are the basis to retrieve ionospheric TEC in this work, a detailed description of the TRSR-2 receiver and its antenna array is given in the following section.

2.4.3. The TRSR-2 GPS receiver

This GPS receiver, which is also called "BlackJack", was engineered and provided by NASA's Jet Propulsion Laboratory (JPL). The TRSR-2 receiver offers three different measurement modes: the default tracking mode which is used for the precise orbit determination, the occultation mode to perform a limb sounding of the atmosphere, and the altimetry mode by which a nadir antenna collects specular reflections of GPS signals from the surface of the oceans. The TRSR-2 is a sixteen-channel receiver configured for a high-low satellite-to-satellite link. The receiver allows a maximum of twelve GPS satellites to be tracked at the same time for orbit determination and up to four GPS satellites for occultation measurements. Besides the main GPS receiver, there is an additional spare TRSR-2 receiver which can only track up to eight satellites at a time. The GPS signals for orbit determination are recorded at a frequency of 0.1 Hz, whereas the occultation measurements have a higher frequency with 50 Hz.

CHAMP employs four antennas for the TRSR-2 receiver: a POD antenna with three choke rings installed on the top side of the satellite, a spare POD antenna and a helix antenna with a 20° downward inclination for occultation measurements at the rear side of the satellite, and a nadir-viewing helix antenna for GPS altimetry. A detailed depiction of the antenna configuration is given in Fig. 4
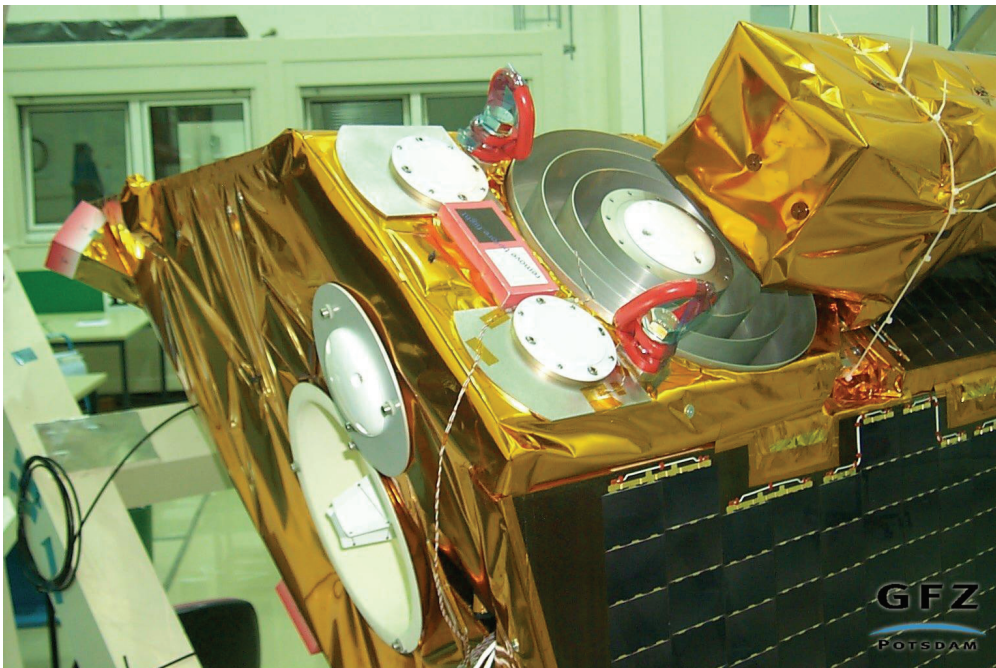

Figure 4: CHAMP GPS antenna configuration (image source: CHAMP website (Lühr, 2010))

3. Analysis

In this section an analysis of the necessary algorithms and procedures is given which constitute the basis of the following TEC retrieval method. This involves the TEC determination from GPS observations, the correction of the GPS observations, the resolution of the carrier phase ambiguities, the estimation of the pseudo-range multipath and the differential code bias of the GPS receiver, as well as a description of the data that is required to accomplish the individual procedures.

3.1. TEC determination from GPS observations

As already stated in section 2.3.3, the observation equations described in equations (10) and (11) can be used to extract ionospheric information by subtracting simultaneous code phase and carrier phase observations. P2-P1 and L1-L2 form the so-called ionospheric combinations P_I and L_I (Blewitt, 1990), which eliminate all non-dispersive terms:

$$P_I \equiv P_2 - P_1 = \Delta_{ion_{P2}} - \Delta_{ion_{P1}} - DCB_S - DCB_R + \Delta\varepsilon_P \tag{12}$$

$$L_I \equiv L_1 - L_2 = \Delta_{ion_{L2}} - \Delta_{ion_{L1}} + N_1\lambda_1 - N_2\lambda_2 + DPB_S + DPB_R + \Delta\varepsilon_L \tag{13}$$

Considering equation (9), equation (12) can be written as:

$$P_I = TEC_P = K\frac{f_1^2 - f_2^2}{f_1^2 \cdot f_2^2}TEC - DCB_S - DCB_R + \Delta\varepsilon_P$$
$$K = 40.3m^3s^{-2} \tag{14}$$

With knowledge of the differential code biases of the receiver and satellite (DCB_R and DCB_S) and the additional noise $\Delta\varepsilon_P$, which is mostly due to multipath effects, equation (14) can be used to determine TEC along the ray path of P1 and P2. Using carrier phase observations, TEC determination is described by:

$$L_I = TEC_L = K\frac{f_1^2 - f_2^2}{f_1^2 \cdot f_2^2}TEC + DPB_S + DPB_R + N_1\lambda_1 - N_2\lambda_2$$
$$K = 40.3m^3s^{-2} \tag{15}$$

Due to the unknown carrier phase ambiguities N_1 and N_2 and the differential carrier biases DPB_R and DPB_S, TEC derived from carrier phase observations is also not absolute. However,

the combination of carrier phase ambiguities and differential carrier biases can be assumed to be constant over a certain period of time. Additionally, the noise and multipath of the carrier phases $\Delta\varepsilon_L$ is in the range of millimetres so that it can be neglected for TEC retrieval. When determining TEC from GPS observations, it is a common approach to combine the advantages of the two observation types by fitting the low noise carrier phase differences into the non-ambiguous code phase differences to resolve the ambiguities of the carrier phases. This fitting procedure is explained in detail in section 3.4.

3.2. GPS data correction

GPS observations generally contain disturbances and erroneous measurements which have to be removed in order to derive TEC. Additionally, there is the problem of so-called cycle-slips. Cycle-slips are discontinuities in carrier phase observations due to a loss of lock of the GPS satellite, which results in an arbitrary change of the carrier phase ambiguities during a satellite track. To achieve a resolution of the carrier phase ambiguities, these discontinuities have to be corrected. Blewitt (1990) introduced an automatic cycle-slip detection and correction algorithm for ground-based GPS data which is also suitable and commonly used for space-based data. This algorithm will be described in the following.

The basic approach of this algorithm is a model of undifferenced carrier phase and code phase data with:

$$L_1 \equiv -\frac{c\,\Phi_1}{f_1} = \rho - I\frac{f_2^2}{f_1^2 - f_2^2} + \lambda_1 N_1 \tag{16}$$

$$L_2 \equiv -\frac{c\,\Phi_2}{f_2} = \rho - I\frac{f_1^2}{f_1^2 - f_2^2} + \lambda_2 N_2 \tag{17}$$

$$P_1 = \rho + I\frac{f_2^2}{f_1^2 - f_2^2} \tag{18}$$

$$P_2 = \rho + I\frac{f_1^2}{f_1^2 - f_2^2} \tag{19}$$

where c denotes the speed of light, Φ_1 and Φ_2 are the phases of the observed carrier waves, ρ denotes the combination of all non-dispersive terms (geometric error, tropospheric propagation error, clock errors), and I includes the ionospheric propagation error and the instrumental biases

of the satellite and the receiver. The above mentioned cycle-slips are integer values denoted by ΔN_i with:

$$(\Delta N_1, \Delta N_2) = (N_1' - N_1, N_2' - N_2) \tag{20}$$

where N_1' and N_2' are the new values of the carrier phase ambiguities (N_i) after the cycle-slip.

3.2.1. Cycle-slip detection in the wide-lane combination

The so-called wide-lane combination of the carrier phases is used to detect cycle-slips, which is defined by:

$$\Phi_\delta \equiv \Phi_1 - \Phi_2 \tag{21}$$

The wide-lane ambiguity N_δ is the difference of the carrier phase ambiguities on both frequencies with:

$$N_\delta \equiv N_1 - N_2 = \frac{L_\delta - P_\delta}{\lambda_\delta} \tag{22}$$

where

$$L_\delta = \frac{f_1 L_1 - f_2 L_2}{f_1 - f_2} \tag{23}$$

$$P_\delta = \frac{f_1 P_1 + f_2 P_2}{f_1 + f_2} \tag{24}$$

$$\lambda_\delta \equiv \frac{c}{f_1 - f_2} \approx 0.862m \tag{25}$$

λ_δ is approximately four times the wavelength of the carrier waves of L_1 and L_2, leading to the naming "wide-lane". The main objective of the detection in the wide-lane combination is to find changes in the N_δ value of continuous observations that exceed a certain threshold, which then denote the cycle-slips. Thereby, N_δ can be interpreted as value for the carrier phase ambiguities with respect to the code phase observations.

From the perspective of the POD antenna, the GPS satellites perform arcs in terms of ray elevation (see Fig. 5). The analysis of the GPS data is therefore aimed at the creation of so-called phase connected arcs, which are continuous sequences of observations of a satellite track without the occurrence of a cycle-slip. The cycle-slip threshold is determined by the root mean square (RMS) error σ_i^2 between the N_δ value of an individual observation and the mean value $\langle N_\delta \rangle$ of the corresponding satellite track. The phase connected arcs are created by calculating an iterative mean value $\langle N_\delta \rangle_i$ and RMS error σ_i^2 using the $N_{\delta\ i}$ values of continuous observations with:

$$\langle N_\delta \rangle_{i+1} = \langle N_\delta \rangle_i + \frac{N_{\delta\ i+1} - \langle N_\delta \rangle_i}{i+1} \tag{26}$$

$$\sigma_{i+1}^2 = \sigma_i^2 + \frac{(N_{\delta\ i+1} - \langle N_\delta \rangle_i)^2 - \sigma_i^2}{i+1} \tag{27}$$

A cycle-slip is detected if the $N_{\delta\ i+1}$ and $N_{\delta\ i+2}$ values of two consecutive observations deviate more than $4\sigma_i$ from the current mean value $\langle N_\delta \rangle_i$. When a cycle-slip is detected, the current arc is closed and a new one is created. If only $N_{\delta\ i+1}$ is above the cycle-slip threshold, this observation is considered as an outlier and the current arc continues. As the σ value needs several observations to be adjusted properly, Blewitt (1990) recommends an initial σ value of 0.5 for each newly created arc. This threshold has to be determined empirically to fit the data of the CHAMP satellite.

3.2.2. Wide-lane phase connection and cycle-slip correction

The $\langle N_\delta \rangle_i$ values of the phase connected arcs are used to test the possibility of reconnecting cycle-slip separated arcs. To create a connection, an adequate integer value for the difference ΔN_δ of the $\langle N_\delta \rangle_i$ values of two consecutive arcs has to be found. Therefore, the data point N with the smallest standard error in the mean $\sigma_N / \sqrt{N-1}$ of the two arcs is used. The required integer offset between the arcs is found by rounding if the smallest standard errors are both less than 0.15 and the difference of the values with the smallest errors is less than 0.3. Otherwise, a connection is rejected. As with the cycle-slip detection, the given thresholds are recommendations which have to be adjusted to fit the analysed data.
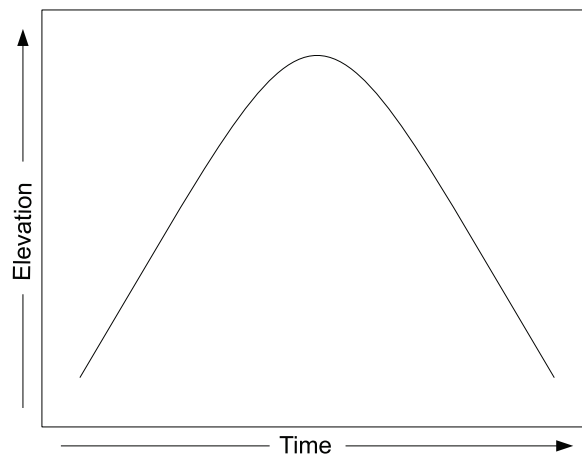

Figure 5: Elevation arc of a continuous GPS satellite track above the CHAMP POD antenna

Having found an appropriate ΔN_δ value, the carrier phase ambiguity differences ΔN_1 and ΔN_2 have to be determined in order to correct the cycle-slips (see equation (20)). The ionospheric combination L_I is considered for that as it can be written as:

$$L_I = L_1 - L_2 = I + \lambda_1 N_1 - \lambda_2 N_2 = I + \lambda_1(N_1 - N_2) + (\lambda_1 - \lambda_2)N_2$$
$$= I + \lambda_1 N_\delta + (\lambda_1 - \lambda_2)N_2 \tag{28}$$

With the difference of L_I before and after the cycle-slip denoted by ΔL_I, ΔN_2 can be determined by:

$$\Delta N_2 = \frac{\Delta L_I - \lambda_1 \Delta N_\delta}{\lambda_1 - \lambda_2} \tag{29}$$

ΔN_1 is calculated as $\Delta N_2 + \Delta N_\delta$, which then offers the possibility to calculate the corrected carrier phase observations of the second arc:

$$L_1' = L_1 - \lambda_1 \Delta N_1 \qquad L_2' = L_2 - \lambda_1 \Delta N_2 \tag{30}$$

3.3. Pseudo-range multipath estimation

The resolution of the carrier phase ambiguities by fitting the carrier phase differences into the code phase differences strongly depends on the level of multipath and noise in the code phase observations. Therefore, it is very desirable to remove these disturbing quantities from the observations. Multipath errors of GPS observations are caused by the superposition of the direct signal with interfering signals in the vicinity of the antenna which are mainly caused by reflections. For the CHAMP POD antenna the maximum multipath error is confined to the dimensions of the satellite body. As already mentioned, the multipath error and additional noise of carrier phase observations are very small and can be neglected when determining TEC. This is different for code phase observations, which can have multipath and noise errors of several metres.

An analysis of the multipath for the CHAMP POD antenna is given in Montenbruck and Kroes (2003), which confirms the presence of pseudo-range multipath errors. To analyse the multipath errors, the so-called multipath combinations were used, which are described by:

$$M_{P1} + \varepsilon_{P1} \approx P_1 - \frac{2}{f_1^2 - f_2^2}(f_1^2 L_2 - f_1^2 L_1) - L_1 - B_{P1} \tag{31}$$

$$M_{P2} + \varepsilon_{P2} \approx P_2 - \frac{2}{f_1^2 - f_2^2}(f_1^2 L_2 - f_1^2 L_1) - L_2 - B_{P2} \tag{32}$$

In these linear combinations the receiver-to-satellite geometry and the ionospheric path delay both are omitted. The carrier phase ambiguities and the differential code biases are combined in the B_{Pi} terms. These offsets can be assumed to be constant during a continuous pass of carrier phase observations. Accounting for the negligible carrier phase multipath and noise errors, the pseudo-range multipath and noise can be determined from these linear combinations if an appropriate offset (B_{Pi}) can be found.

3.4. Resolution of the carrier phase ambiguities

A resolution of the carrier phase ambiguities can be approximated by "shifting" the carrier phase differences (L_I see equation (13)) into the non-ambiguous code phase differences (P_I see equation (12)). This however requires cycle-slip free arcs of GPS observations, which can be created with the algorithm described in section 3.2. To determine the shifting value S_I for the carrier phase differences, the difference of the mean value of the carrier phase differences $\langle L_I \rangle$ and code phase differences $\langle P_I \rangle$ can be calculated on a per arc basis with:

$$S_I = \langle P_I \rangle - \langle L_I \rangle \tag{33}$$

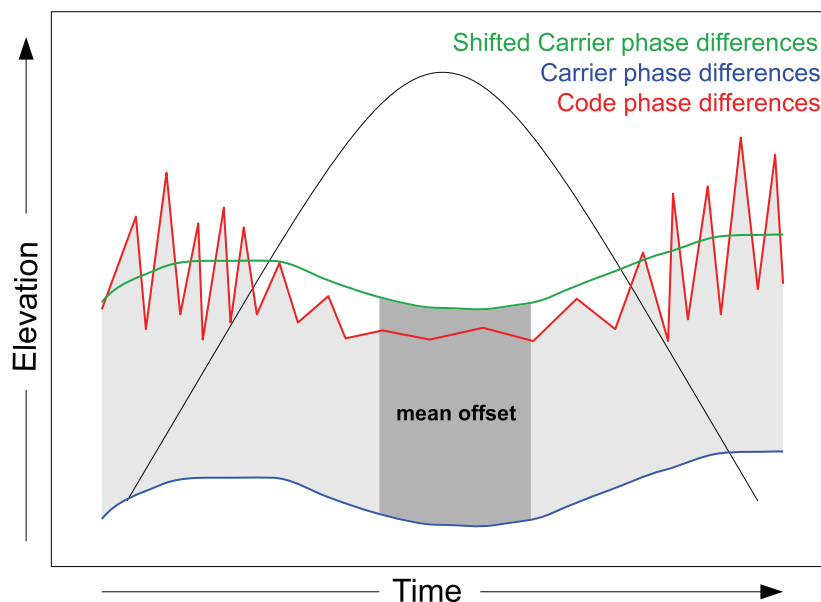This so-called "carrier-to-code-shifting" approach is also visualized with a schematic example in Fig. 6.

Figure 6: Resolution of carrier phase ambiguities by "carrier-to-code-shifting"

3.5. Receiver differential code bias estimation

The receiver differential code bias (DCB) is one of the terms in equation (14) that has to be estimated in order to retrieve TEC. The DCB of a GPS receiver is mainly caused by path delay differences during the processing of P1 and P2 in the receiver hardware. In Heise et al. (2003) a model-based approach was used to calibrate the receiver DCB. This approach is however inappropriate for a near real-time retrieval of TEC due to the additional effort of calculating a model of the ionosphere. A more suitable approach for the receiver DCB estimation is described in Syndergaard (2007). The therein described procedure is based on the assumption that TEC is equal for paired simultaneous GPS observations. A schematic illustration of the corresponding satellite geometry is given in Fig. 7. Accounting for the ray elevation, the relation of the paired observations is described by:

$$TEC_A \cdot M(\theta_A) = TEC_B \cdot M(\theta_B) \tag{34}$$

where

$$TEC_i = T\tilde{E}C_i + DCB_T + DCB_R + n_i \tag{35}$$

$$M(\theta) = \frac{sin\theta + \sqrt{\tilde{r}^{-2} - cos^2\theta}}{1 + \tilde{r}^{-1}} \tag{36}$$

with

TEC_i TEC of the paired observations,

$T\tilde{E}C_i$ Code-levelled carrier phase TEC of the paired observations,

DCB_T Differential code bias of the transmitter,

DCB_R Differential code bias of the receiver,

n_i Remaining error of the paired observations,

M Geometric mapping function,

θ Ray elevation, and

$\tilde{r}$ Radius of the Earth / (Radius of the Earth + CHAMP altitude).
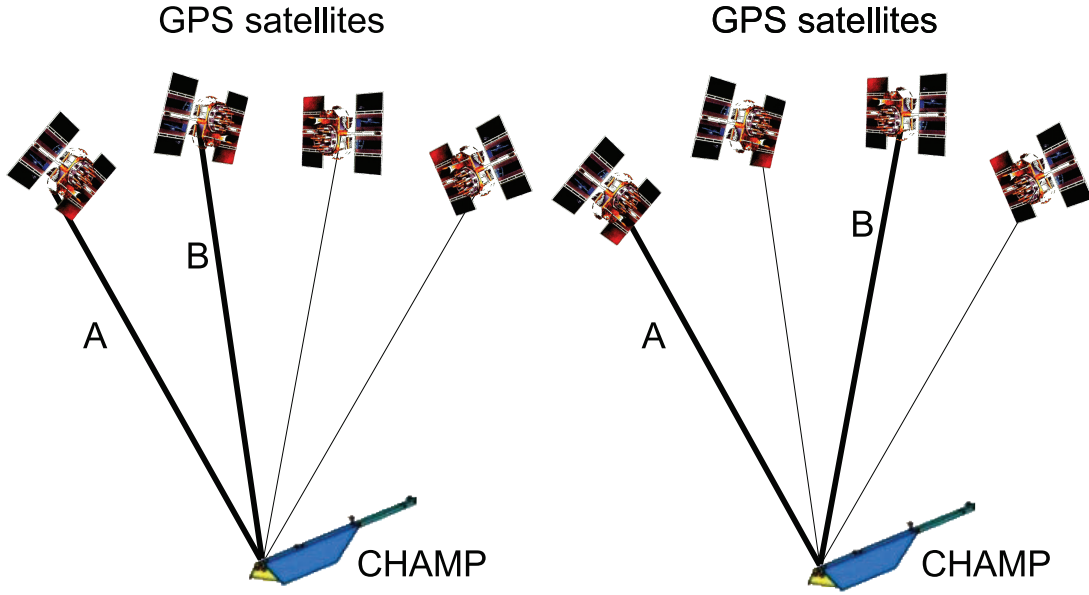
Figure 7: Constellation of paired observations for the receiver DCB estimation

M is a geometric mapping function of the ray elevation θ described in Foelsche and Kirchengast (2002). Rewriting equation (34) with respect to equation (35) results in:

$$T\tilde{E}C_A M(\theta_A) + DCB_T M(\theta_A) + DCB_R M(\theta_A) + n_A M(\theta_A)$$

$$= \qquad (37)$$

$$T\tilde{E}C_B M(\theta_B) + DCB_T M(\theta_B) + DCB_R M(\theta_B) + n_B M(\theta_B)$$

Assuming that the error of both observations is equal ($n_A M(\theta_A) - n_B M(\theta_B) = 0$), all paired observations of a day can be used to create a system of linear equations in the form of $y = Ax$ with:

$$\begin{pmatrix} (T\tilde{E}C_A(1) + DCB_T(1))M(\theta_A)(1) - (T\tilde{E}C_B(1) + DCB_T(1))M(\theta_B)(1) \\ (T\tilde{E}C_A(2) + DCB_T(2))M(\theta_A)(2) - (T\tilde{E}C_B(2) + DCB_T(1))M(\theta_B)(2) \\ \dots \\ (T\tilde{E}C_A(l) + DCB_T(l))M(\theta_A)(l) - (T\tilde{E}C_B(l) + DCB_T(l))M(\theta_B)(l) \end{pmatrix} = \begin{pmatrix} M(\theta_B)(1) - M(\theta_A)(1) \\ M(\theta_B)(2) - M(\theta_A)(2) \\ \dots \\ M(\theta_B)(l) - M(\theta_A)(l) \end{pmatrix} * DCB_R \quad (38)$$

The receiver DCB is eventually derived by applying the method of least squares to the system of linear equations in the form of $x = (A^T A)^{-1} A^T y$ and results in:

$$DCB_R = \frac{\sum (M(\theta_B) - M(\theta_A))(\widehat{T\tilde{E}C_A}M(\theta_A) - \widehat{T\tilde{E}C_B}M(\theta_B))}{\sum (M(\theta_B) - M(\theta_A))^2} \quad (39)$$

where $\widehat{TEC_i}$ denotes the sum of the code-levelled carrier phase TEC and the DCB of the transmitter. Due to the application of the geometric function of the ray elevation, the resulting receiver DCB represents a weighted average of the paired observations.

3.6. Required data

The above described algorithms require basically four different types of data to achieve a TEC retrieval: CHAMP GPS observations, orbit information of the CHAMP satellite, orbit information of the GPS satellites, and differential code biases of the GPS satellites.

3.6.1. CHAMP GPS data

GPS observations of the precise orbit determination antenna aboard CHAMP are available from the Information System and Data Center (ISDC) of the GFZ. CHAMP GPS data is given in the RINEX standard 2.10 (Gurtner, 2007) at a data rate of 10 seconds and involve L1, L2, P1, P2, and C1 (C/A) observations, as well as the signal-to-noise ratios S1 and S2 of L1 and L2, respectively. Pseudo-ranges are given in metres, whereas carrier phases are presented in wave cycles and have to be converted to metres to be analysed. The time of the observations is given in GPS seconds starting January 6, 1980, 12 am. Each CHAMP GPS RINEX file contains the data of a single day to be compatible with the GPS orbit data.

3.6.2. CHAMP orbits

CHAMP orbit data is mainly necessary for the calculation of the altitude of the CHAMP satellite and also for determining the elevation and azimuth angles of the GPS observations during TEC retrieval. The orbits of the CHAMP satellite are predictions given in the CHORB format (König et al., 2001). The orbit data contains the position and velocity of the CHAMP satellite given in the earth-fixed reference frame *WGS 84* at a data rate of 60 seconds. The time of the orbit data is indicated by the Modified Julian Day (MJD) starting January 1, 2000, 12 pm and additionally elapsed seconds. The CHAMP orbit files contain the orbit predictions of the current day and the following 3 days with decreasing precision. Like CHAMP GPS data, orbit information is available from the ISDC.

3.6.3. GPS satellite orbits

The orbits of the GPS satellites are also required to calculate the elevation and azimuth angles of the GPS observations. GPS orbit data is available from the IGS website[1] and comes in the SP3-format (Spofford and Remondi, 1991) on a daily basis. The orbit files contain the position and velocity of all GPS satellites at a data rate of 15 minutes in the WGS 84 reference frame. The time declaration of the orbit data is GPS time represented in a *YYYY MM DD HH MM SS*-format similar to the ISO 8601 date and time notation.

3.6.4. GPS satellite differential code biases

The differential code biases of the GPS satellites represent a crucial quantity in determining TEC. On the one hand they are one of the measurement dependent terms in the ionospheric combinations in equations (12) and (13) and on the other hand they are required for the estimation of the receiver differential code bias. GPS satellite biases are for example produced by the JPL and also available from the IGS[2]. The DCB values are provided on a daily basis as they can be assumed to be stable for the period of day. GPS satellite biases from the IGS are presented in terms of nanoseconds and have to be converted to TECU in order to be processed. This conversion is described by:

$$1 \, ns \equiv \frac{f_1^2 \cdot f_2^2}{K(f_1^2 - f_2^2)} \, c \cdot 10^{-9} \, TECU$$

$$1 \, ns \approx 2.8539 \, TECU$$

(40)

---

[1]http://igscb.jpl.nasa.gov/components/prods_cb.html, retrieved July 20, 2010
[2]ftp://igs.ensg.ign.fr/pub/igs/products/ionosphere/, retrieved July 20, 2010

4. Conception

The following section describes the conception for the implementation of the TEC retrieval. As one of the main objectives of the intended retrieval method is a near real-time calculation of TEC, the conception aims for the creation of a single program that automatically calculates all necessary processing steps. The sequence of these required steps results in the general application flow of the TEC retrieval which forms the basis for the then followed description of the automated TEC determination.

4.1. Application flow of the TEC retrieval

The fundamental application flow of the TEC retrieval procedure arises directly from the algorithms and data types described in section 3 and is depicted in a flow chart in Fig. 8.
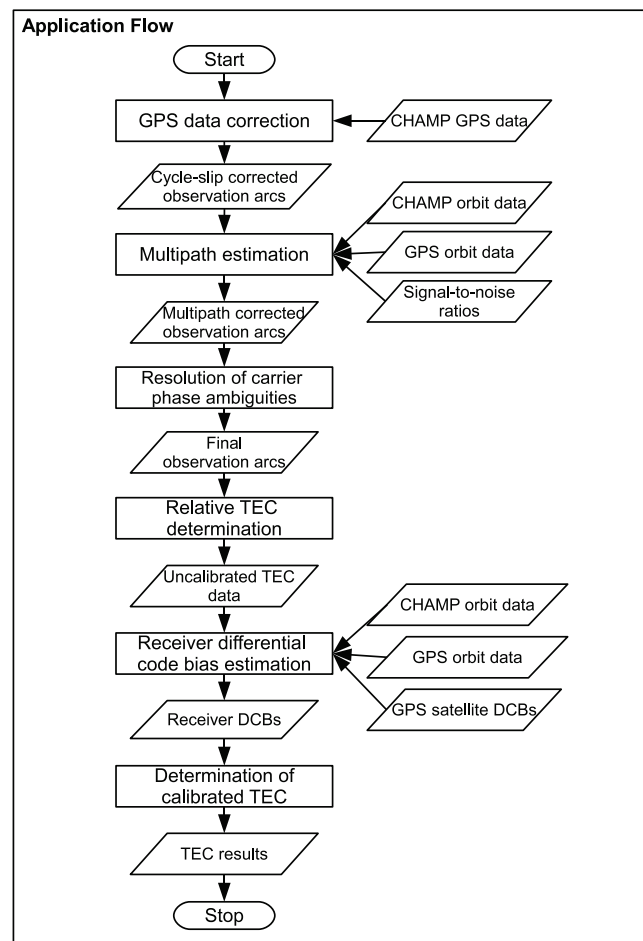

Figure 8: Application flow of the TEC retrieval procedure

4.2. Automated TEC determination

The conception for the implementation of an automated TEC determination begins with a number of preliminary considerations which are crucial for the later implementation. Afterwards, the usage of the program is explained as well as a specialized and adapted flow for the automation including a detailed description of the particular parts of the TEC determination. This is followed by the conception for the output of the TEC retrieval. The section is concluded with the conception for the structure of the automated TEC determination program.

4.2.1. Preliminary considerations

The implementation of the TEC retrieval program is not completely build from scratch. For the GPS data correction and the resolution of the carrier phase ambiguities an adaption of the Fortran 77 routines from Stolle (2004) is used which were developed for processing GPS observations of the CHAMP occultation antenna. Due to this adaption, Fortran 77 is the intended programming language for the later implementation. Fortran 77 is limited to structural programming, which has its shortcomings in comparison to modern object-oriented programming with languages such as C++ or Java. However, it provides a very decent execution speed that is needed for a near real-time calculation of TEC. The choice of Fortran 77 has a number of implications on the conception of the automated TEC determination which will be described in the following sections.

4.2.2. Usage

As the TEC determination process is basically a sequence of several calculation steps without the need for any user interaction in between, the implemented program is mostly suitable to be executed from a command-line interface. This fits the common usage of Fortran and also offers the possibility of integrating the TEC determination program into a script for an automated or regular execution. To start its work, the automated TEC determination program needs one vital piece of information, which is the desired period of time for the processing. The most suitable way of providing this information are command-line parameters passed to the program at its execution. As Fortran is a compiled programming language, changing any settings of the TEC determination process requires a recompilation of the program, which is not appropriate in practice. Therefore, providing a possibility for an external configuration of the TEC determination process is intended. The designated usage of the TEC determination program is depicted in a use case diagram in Fig. 9.
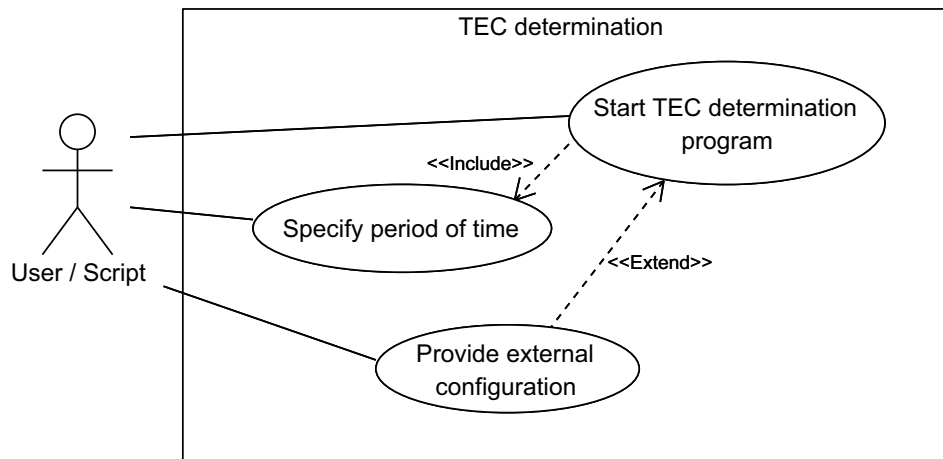
Figure 9: Use case diagram of the TEC determination

4.2.3. Flow

The flow of the automated TEC determination requires a number of additional steps which mainly refer to retrieving and providing required data automatically to the corresponding algorithms. The combination of the additional data retrieval steps and the TEC determination algorithms, as well as the detailed data flow is depicted in an activity diagram in Fig. 10.

Determination of the processing time period

Before any of the required files can be retrieved and provided, the period of time for the TEC retrieval has to be determined from the information provided by the command-line parameters. Since all data types are provided on a daily basis, the TEC determination is also intended to be performed by the day to conform with the data. Therefore, the dates of all days in the given period of time have to be determined.

Configuration setup

The determination of the dates for the TEC retrieval is followed by the configuration of the processing. As described in section 4.2.2, configuration data can be provided externally and will be evaluated if possible. Otherwise, a default configuration is applied. The configuration possibilities should include the paths of the input and output data, TEC determination parameters, and the possibility to enable or disable certain types of output (see section 4.2.4).

Figure 10: Activity diagram for the application flow of the TEC determination

Data retrieval

Having determined the days for the processing and set up the configuration, the next step is to locate and retrieve all required input data (CHAMP GPS observations, CHAMP orbits, GPS orbits, GPS satellite DCB). For a daily based TEC determination it would actually be sufficient to provide the data of the current day. However, it can be assumed for almost each day that there are data arcs situated on the edge of the day. Therefore, it would be desirable to also provide the data of the previous and the following day to be able to analyse these arcs.

GPS data correction

The actual first step in the TEC determination process is the correction of the GPS observations, hence a cycle-slip detection and correction based on the algorithms described in section 3.2, resulting in continuous data arcs which form the basis for all following processing steps. The Fortran 77 routines from Stolle (2004) conform exactly to the algorithms with an addition for the determination of ΔL_I (see equation (29)), the difference of the carrier phase differences before and after a cycle-slip. The calculation of ΔL_I is based on a polynomial extrapolation from the first to the second of two cycle-slip separated arcs, which is also used to test the connectivity of the arcs. This approach is also suitable for the data arcs of the CHAMP POD antenna. The adaption of the Fortran 77 routines for the GPS data correction refers mostly to the integration of the routines into the automatic processing flow and the adjustment of the detection parameters.

Multipath estimation

Before the carrier phase ambiguities are resolved, the pseudo-range multipath estimation is applied to the code phase observations. The deciding part in the multipath estimation using the linear combinations in equations (31) and (32) is to adjust the offsets (B_{Pi}) on a per-arc basis of the GPS satellites to achieve a zero mean left-hand side of the equations. From the perspective of processing speed, this can be accomplished in the simplest case by calculating the mean value of all multipath combinations of a single arc. This approach is similar to shifting the carrier phase differences into the code phase differences and results in a very balanced distribution of the multipath values (see Fig. 11(a)). As multipath errors are mostly constrained to low elevations ($< 30°$), errors that occur in high elevations ($> 60°$) should be very small, consisting only of noise. Therefore, a weighted average of the multipath combinations is more suitable than the mean value, shifting the carrier phase differences closer to the low noise code phase differences (see Fig. 11(b)), which results in more precise multipath values. To create a weighting,
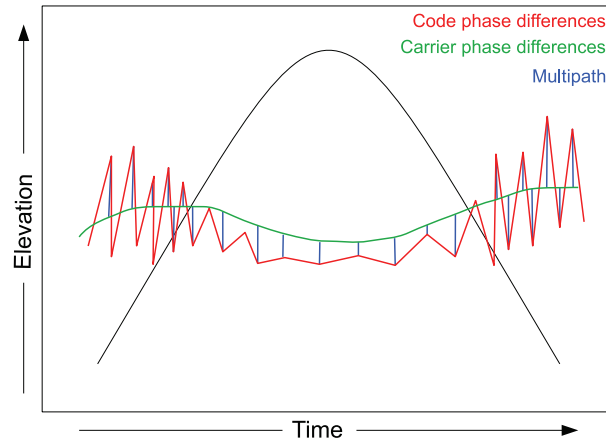
(a) Multipath estimation using the mean value
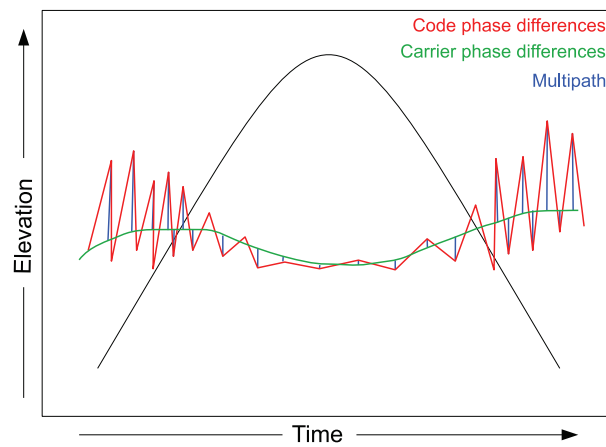
(b) Multipath estimation using a weighted average

Figure 11: Multipath estimation comparison

the signal-to-noise ratios of L1 and L2 are intended to be used as they are well correlated to the elevation of the GPS observations.

The multipath estimation based on the approach described above has one major limitation. The quality of the estimation approach strongly depends on the presence of low noise code phase observations to find an appropriate shifting value for the carrier phase differences. If there are no low noise observations in an arc, the multipath values are likely to become unstable. To overcome this problem, the multipath values of a certain period of time are averaged with respect to ray elevation and azimuth. Additionally, the estimated multipath is actually multipath and noise. Averaging the multipath values also implicates a separation of multipath and noise since noise can be assumed stable over certain period of time.

Resolution of the carrier phase ambiguities

The resolution of the carrier phase ambiguities denotes the last step in the processing flow before TEC can be retrieved from the carrier phase observations. The corresponding Fortran 77 routine from Stolle (2004) complies with the descriptions in section 3.4 and offers the additional possibility of using the median value instead of the mean value to shift the carrier phase differences into the code phase differences. The integration into the processing flow denotes the major part in adapting the existing routine to the automated TEC determination.

Calculation of relative TEC

Having resolved the carrier phase ambiguities, equations (12) and (13) are combined to calculate TEC from the code-levelled carrier phase observations with:

$$TEC_{rel} = (L_1^{code} - L_2^{code}) \frac{f_1^2 \cdot f_2^2}{K(f_1^2 - f_2^2)} \qquad (41)$$

In this equation the code-levelled carrier phase observations L_1^{code} and L_2^{code} have to be interpreted as code phase observations without noise, hence the $\Delta\varepsilon$ term from equation (12) is eliminated. Furthermore, the remaining differential code biases of the receiver and satellite are not considered so that a calculation of relative TEC is achieved. The receiver DCB is estimated in the next processing step using the relative TEC values and the GPS satellite DCB data from the JPL.

Receiver differential code bias estimation

To estimate the receiver DCB with the approach described in section 3.5, it is necessary to choose an appropriate minimum elevation. As the noise level of the observations is well correlated with the ray elevation, it is convenient to consider only observations with a minimum elevation of $45°$ for the calculation of the DCB. The deciding requirement for finding the target value of the DCB is the absence of negative TEC values after the addition of the receiver and satellite DCB (see equation (14)). If there are negative TEC values, the receiver DCB has to be adjusted. One approach is a recalculation of the DCB with a higher minimum elevation of the observations since a decreased noise level is expected for high elevations. Another approach of finding the target value of the receiver DCB is to increase the initial DCB value gradually until no negative TEC values occur.

Regardless of weather the DCB is estimated by increasing the elevation limit or adjusting the DCB value itself, finding an acceptable value that prevents the occurrence of negative TEC values cannot be guaranteed due to inaccuracies in the multipath estimation and the calculation of the elevation angles, which could cause outliers in the relative TEC values. When handling this issue with the approach of increasing the elevation limit, it has to be considered that the denominator of equation (39) mainly represents the squared difference of the sine of the elevation angles, which gets very close to zero if all considered observations have an elevation near $90°$. This could lead to unstable results if there are relative TEC values that do not follow the assumption of low noise data in high elevations. Additionally, it has to be considered that there could be phase connected data arcs which do not contain any high elevation observations. In the worst case, it would not be possible to calculate the receiver DCB. The second approach of adjusting the DCB value is more suitable for detecting outliers since the number of negative TEC values converges to a certain amount when the receiver DCB is increased. Finding appropriate termination conditions for the increase is crucial for the implementation of the receiver DCB estimation to prevent unstable results.

Results

Although it would be easily possible to provide absolute TEC values as the main result of the automatic TEC determination by adding the receiver and satellite DCB to the relative TEC values, it is intended to separately provide only relative TEC values and the receiver DCB. The provision of absolute TEC values would be confined to the usage of the JPL GPS satellite DCB data. Furthermore, the usage of the JPL GPS satellite DCB to provide absolute TEC values implicates a dependence on the reliability of these external data, which is not desired. To better characterize the TEC results, the corresponding base data such as the GPS time stamp, the GPS satellite, the original GPS observations, and the orbit position of the CHAMP satellite and the GPS satellite should be provided. It is also intended to provide an additional quality index for the receiver DCB to estimate its applicability.

4.2.4. Output

When all processing steps have finished, the results of the TEC determination are intended to be stored permanently for further use. Since the TEC determination is done by the day, the output should also be created on a daily basis. The main output file for the results of the TEC determination will be a plain text file with the results listed in the form of a table. At the

beginning of the file, a header section with a description of the given data is intended to clarify the origin, properties, and usage of the data. Afterwards, the results of the day will be given in continuous order to be consistent with the structure of the input data. A text output is very convenient for the further use, evaluating the TEC results solely by written numbers can be difficult however. This applies to the TEC results, but especially to the results of the receiver DCB and multipath estimation. Therefore, additional graphical output is intended to visualize the results of the TEC determination, the receiver DCB estimation, and the multipath estimation.

Fortran 77 does not feature facilities for the creation of graphics. However, the language offers the possibility to call external programs, which will be utilized for creating graphical output. The variety of programs that can be used from a command-line interface to automatically create appealing graphics in a moderate period of time narrows down to *Gnuplot*. Gnuplot is a freely distributed multi-platform plotting program that is mainly intended to be used from a command-line interface to visualize data in a variety of plot types which can be saved to a number of different file formats. Besides an interactive mode, the program can be used with externally provided data to create plots. This feature is intended to be used to automatically create the data to be plotted with Fortran, which is then provided to Gnuplot to create graphical output of the TEC determination results. To illustrate the intended creation of graphical output using Gnuplot, a sequence diagram is depicted in Fig. 12.
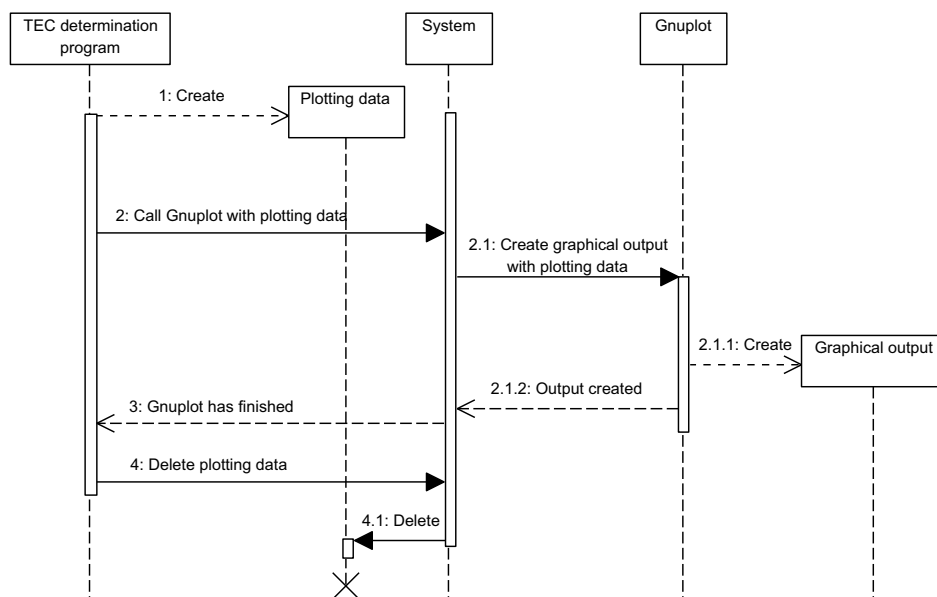

Figure 12: Creation of graphical output using Gnuplot.

4.2.5. Structure

Since Fortran 77 supports neither classes nor user-defined data types (data structures), an object-oriented data model or something similar cannot be accomplished for the implementation of the automatic TEC determination. All data has to be managed on the basis of the built-in data types and arrays of these types. To make the implementation manageable and clear, the automatic TEC retrieval program is intended to have a modularized structure to split the different processing steps of the TEC determination into separate manageable components (modules) which encapsulate a specific task of the program. The intended modularization is depicted in a component diagram in Fig. 13.

The determination of the processing time period and the configuration setup are intended to be contained in a configuration module which requires two interfaces. The first interface refers the command-line variables, which have to be provided by the user of the program or a script, respectively. The second required interface refers to the provision of external configuration data, which is optional however. The configuration module also provides an interface for the dates in the time period for the TEC determination which is required by the module for data input. The data input module combines all processing steps which are necessary to retrieve the required data, and it provides interfaces to the different data types used by the processing algorithms. GPS observation data is required by the module for the GPS data correction, which in turn provides an interface to the cycle-slip corrected GPS data arcs. The module for the multipath estimation requires these data arcs, as well as the CHAMP orbit data and the GPS satellite orbit data for elevation and azimuth calculation, which are provided by the data input module. The resolution of the carrier phase ambiguities is also encapsulated in a module that requires the cycle-slip and multipath corrected data arcs provided by the multipath estimation module. Another module for the calculation of relative TEC requires the cycle-slip corrected carrier phase observations and provides relative TEC values. The receiver DCB estimation is contained in a module which requires these relative TEC values and GPS satellite DCB values, which are provided by the module for data input, as well as CHAMP orbit data and GPS satellite orbit data for elevation calculation. The textual output is included in the data output module which requires relative TEC values, the receiver DCB, and the initial GPS observation data. There are also modules to encapsulate the creation of the graphical output (plotting). Each plotting module requires the corresponding type of result from the TEC processing.
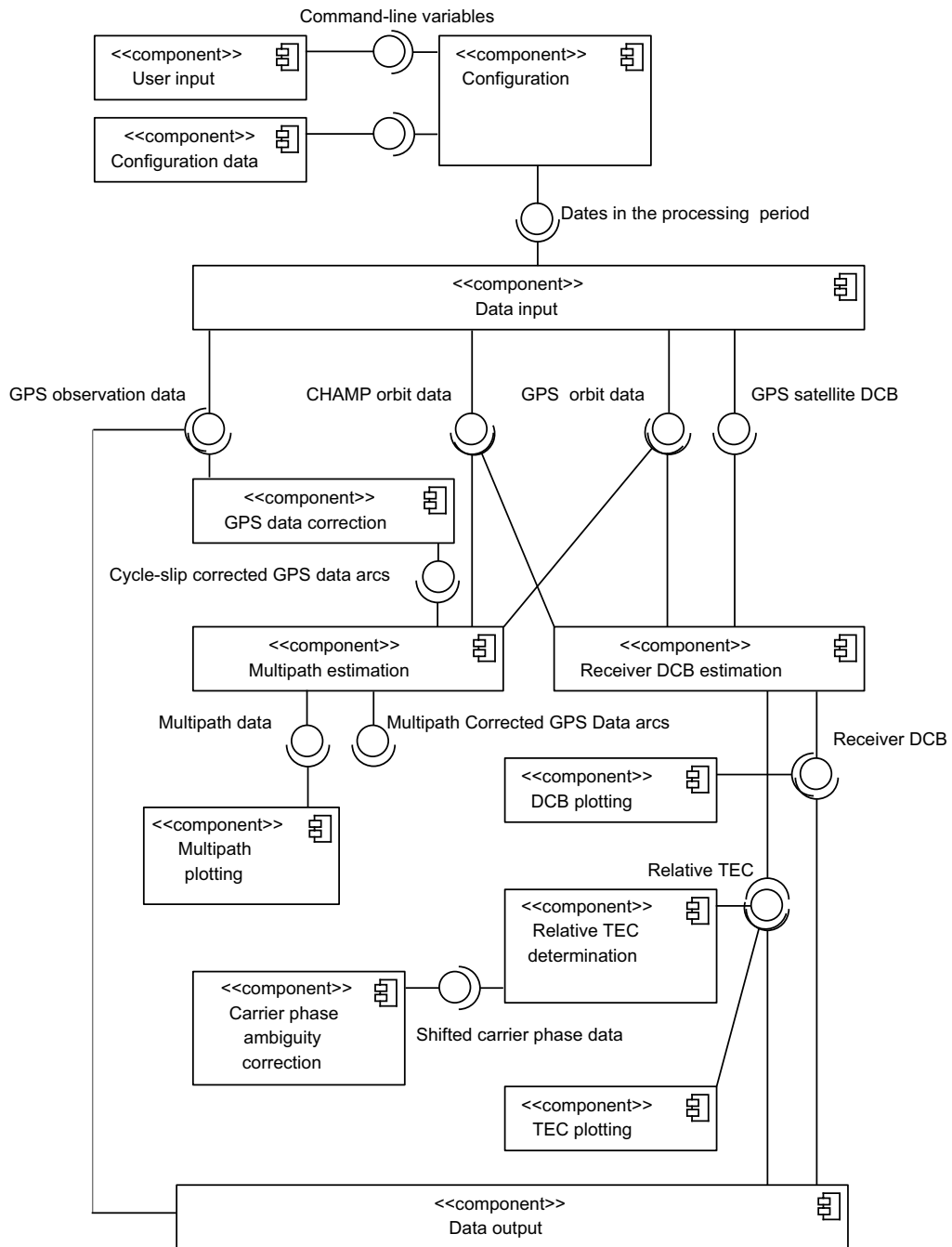
Figure 13: TEC retrieval modularization. The ball and socket notation for the interfaces always denotes a dependency between the modules.

5. Implementation

This section describes the concrete implementation of the TEC determination procedure which is referred to as *TEC processing* for the rest of this section. The description starts with a number of necessary technical prerequisites and the fundamental properties of the implementation. Afterwards an overview is given which is followed by a detailed explanation of the specific parts of the implementation.

5.1. Prerequisites and properties

The implementation of the TEC processing is generally aimed at Linux and UNIX-like operation systems, but can also be compiled on Windows operation systems. For program compilation the free *g77* compiler from the *GNU Compiler Collection (GCC)* is used. Since g77 is not available from GCC 4.0 and above, the program can also be compiled with the *gfortran* compiler. Besides Fortran, Gnuplot in version 4.2.6 is used for the implementation as a means of creating graphical output of the results of the TEC processing. The implementation uses a working directory named *TEC_PROCESSING* that contains the executable program file and an additional configuration file which will be explained in the course of this section. By default, the working directory contains sub-directories for input and output data, named *data* and *results*, respectively.

5.2. TEC processing

The implementation of the TEC processing is realized with a main Fortran `PROGRAM` routine called **tec_proc_main** in the file *tec_proc_main.for*. The intended modularization of the implementation, which was described in section 4.2.5, is realized by Fortran `SUBROUTINES` for every step in the processing flow. The subroutines are named after their corresponding purpose and stored in separate files. The resulting executable of the automatic TEC processing is called **tec_proc**. To start with an overview of the implementation, the application flow of the entire TEC processing is depicted in Fig. 14, which uses dotted rectangles to illustrate the main program loops.

As the implementation does not feature an object-oriented data model with corresponding methods to act on data and provide interfaces, the concept of interfaces requiring and providing data described in section 4.2.5 cannot be implemented directly. All required data is passed to a particular subroutine which then returns the results of its processing. Thereby, **tec_proc_main** serves as a means of a global interface to all subroutines by storing temporary data and results
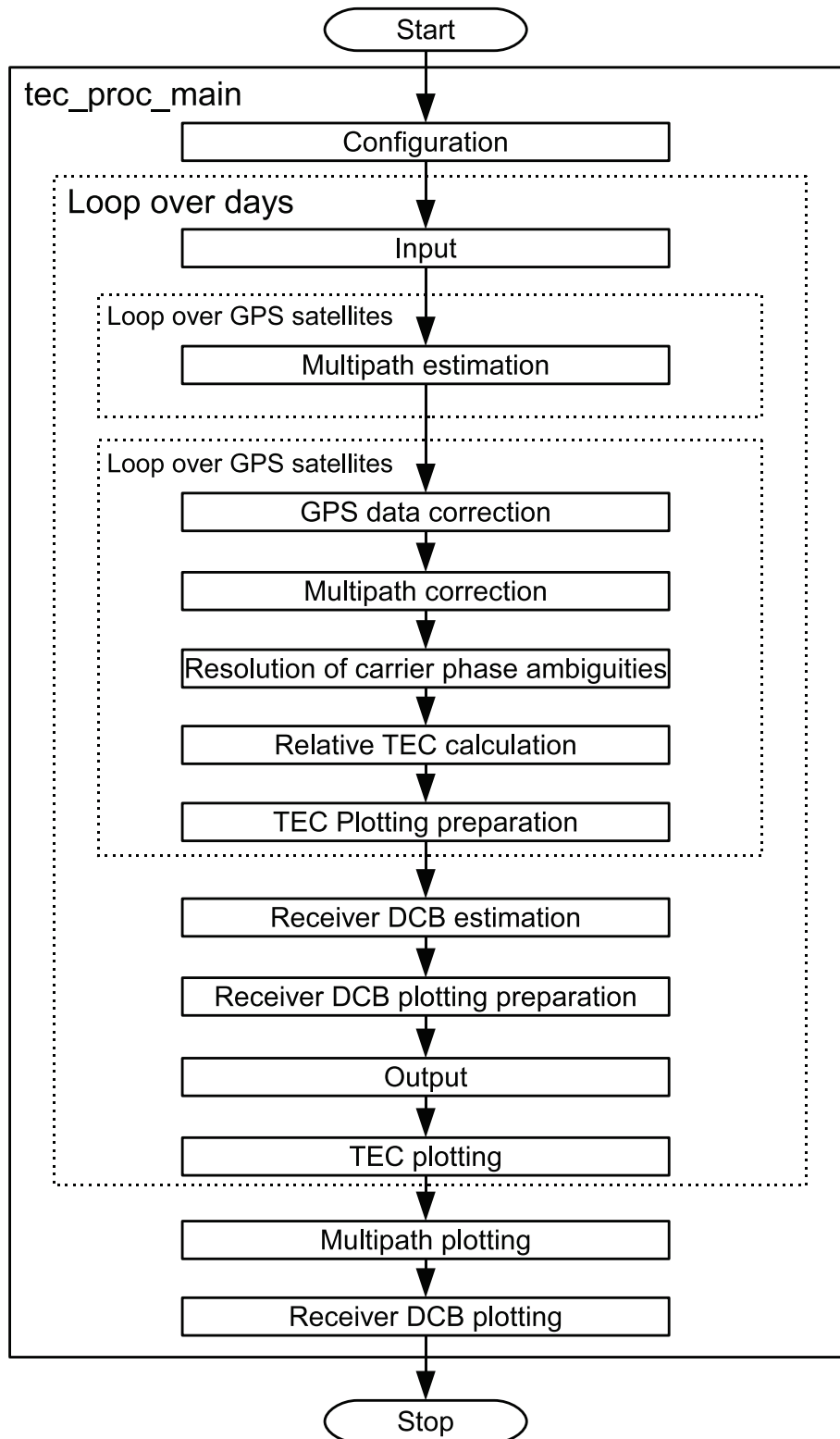
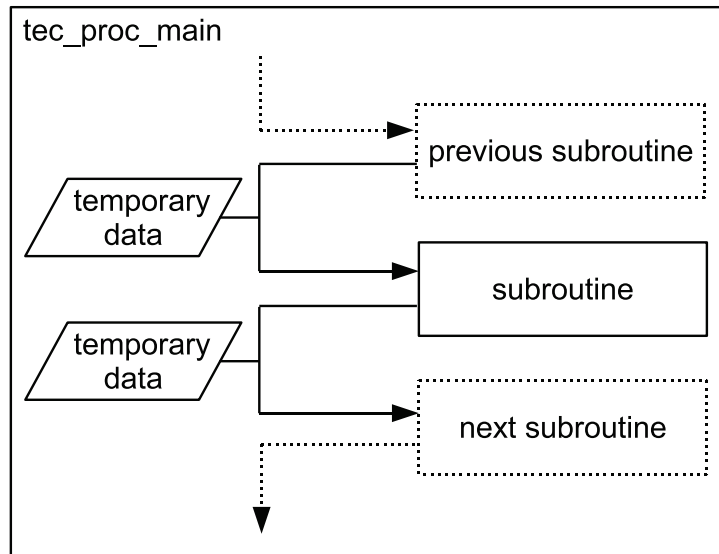Figure 14: Complete application flow of the TEC processing implementation

Figure 15: General data flow of the implementation

and transferring them to the subsequent subroutines. The general data flow of the implementation is depicted in Fig. 15. The following sub-sections contain a number of flow charts to explain the application flow of the implementation in detail. Due to the lack of objects and data encapsulation, a vast number of different data arrays is passed to and returned from a subroutine in many cases. For reasons of clarity, the internal data flow is omitted in all of these flow charts.

5.2.1. Configuration

To achieve an automatic processing, the period of time for the TEC determination has to be provided to the executable file. This is implemented by four command-line variables for the day of the year (DOY) and year of the first day and the DOY and year of the last day in the desired period of time, for example `./tec_proc 1 2007 365 2007`. The subroutine **tec_proc_ command_line_ args** receives these four variables and checks their validity. If all variables contain valid values, the subroutine creates a list with the DOY and year of all days in the specified period of time. Otherwise, the TEC processing ends. The list of dates (DOY and year) is used to locate the required input data since each data type of the CHAMP TEC retrieval is named after a pattern that contains the DOY and year. The subroutine additionally determines the number of days, which is used to create a loop over the days to be analysed during the TEC determination. The implementation of the TEC processing is essentially based on a number of nested loops with the loop over the days at the highest level.

```
                              ╭─────────╮
                              │  Start  │
                              ╰─────────╯
                                   │
   ┌───────────────────────────────┼──────────────────────────┐
   │ tec_proc_main                 ▼                           │
   │                                                           │
   ╱────────────╱       ┌──────────────────────────────────┐  │
   │Commandline │──────▶│    tec_proc_commandline_args      │  │
   │parameters  │       └──────────────────────────────────┘  │
   ╱────────────╱                  │                           │
   │                               ▼                           │
   │                          ◇─────────◇      no              │
   │                         ◇ Parameters ◇──────────┐         │
   │                          ◇  valid?  ◇           │         │
   │                           ◇───────◇             │         │
   │                               │ yes             │         │
   │                               ▼                 │         │
   ╱────────────╱       ┌──────────────────────┐    │         │
   │tec_proc.cfg│──────▶│ tec_proc_configuration│    │         │
   ╱────────────╱       └──────────────────────┘    │         │
   │ ┌ Loop over days ─────────────┼──────────────┐ │         │
   │ ┊                             ▼              ┊ │         │
   │ ┊         yes            ◇──────────◇        ┊ │         │
   │ ┊      ┌───────────────◇  All days  ◇        ┊ │         │
   │ ┊      │               ◇ processed? ◇        ┊ │         │
   │ ┊      │                 ◇────────◇          ┊ │         │
   │ ┊      │                     │ no            ┊ │         │
   │ ┊      │                     ▼               ┊ │         │
   │ ┊      │          ┌──────────────────────┐  ┊ │         │
   │ ┊      │          │  TEC determination    │  ┊ │         │
   │ ┊      │          │  for the current day  │  ┊ │         │
   │ ┊      │          └──────────────────────┘  ┊ │         │
   │ └──────┼──────────────────────────────────┘ │         │
   │        │                     ▼                 │         │
   └────────┴─────────────────────┼─────────────────┘         │
                                   ▼                           
                              ╭─────────╮
                              │  Stop   │
                              ╰─────────╯
```
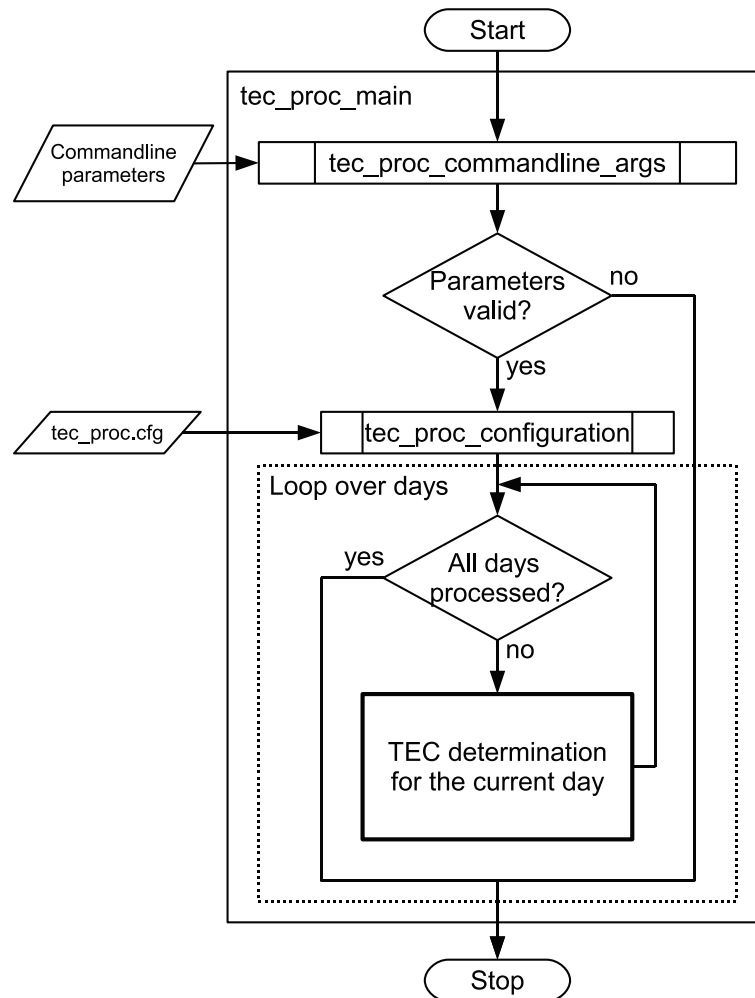
Figure 16: Flow chart for the configuration of the TEC processing.

The actual configuration of the TEC processing is carried out by the subroutine **tec_proc_configuration**. The TEC retrieval can be set up with an external configuration file named *tec_proc.cfg*, which provides a number of options to change the settings of the TEC determination without the need of recompiling the program. The file allows to specify the input and output directories of the TEC retrieval, processing parameters, as well as a number of variables to enable or disable output creation. An explanation of the available configuration options is given in the section of the particular subroutine. The configuration options are also summarized in Table 3 in Appendix A. To illustrate the configuration of the implementation and its position during the TEC processing, a flow chart is given in Fig. 16 which focusses only on the related subroutines.

5.2.2. Input

Inside the main program loop, the TEC processing of a day starts by reading in all necessary input files with the subroutine **tec_proc_input**. The base path of the input files is determined by four configuration variables for the directories of the different data types with *leo_rinex_dir*, *leo_orbit_dir*, *gps_orbit_dir* and *gps_dcb_dir*. Additionally, there is the *input_by_year* configuration variable, which specifies whether the input directories have sub-directories for different years. The name of the particular input file is generated from the DOY and year in conjunction with the specific naming pattern of the data type. The complete path of the CHAMP RINEX files results for example in

<div align="center">

`leo_rinex_dir/`**`year`**`/CH-OG-1-SST+`**`year_doy`**`_00_M.9.rnx`

or

`leo_rinex_dir/CH-OG-1-SST+`**`year_doy`**`_00_M.9.rnx`.

</div>

The RINEX file is also the main input file. The time stamps and data rate of this file is the reference for all other data types. As the CHAMP orbit file and the GPS satellite orbit file both have a different data rate and time format, there is a number of time conversion routines stored in *tec_proc_util.for*. Furthermore, the orbit positions of the CHAMP satellite and the GPS satellites are interpolated to the time stamps of the GPS observations using a cubic spline. The ray elevation and azimuth angles of the GPS observations, which are required for the estimation of the receiver DCB and multipath, are also calculated in **tec_proc_input** and later passed to the corresponding subroutines to avoid a recalculation. Besides the data of the current day, **tec_proc_input** also attempts to read in the data of the previous and the following day in order to be able to analyse data which lie on the edges of the current day. If one of the current days' files is missing or invalid, the whole day is skipped for the TEC determination. If there are missing or invalid files of the previous or following day, the TEC processing continues without that data.

After the input data has been read in and all conversions and interpolations have been done, all data is separated by GPS satellite since the subsequent processing algorithms expect data of one GPS satellite. This separation implicates a loop over the GPS satellites for the further steps of the TEC processing (see Fig. 17). One of the most important decisions for the remaining parts of the implementation is to save only the data of one GPS satellite at a time. With a maximum of 31 GPS satellites to be analysed, this decision helps to confine the memory consumption of the program to a moderate amount. However, this approach also has a number of implications on the particular processing steps, which are explained in the corresponding sections.
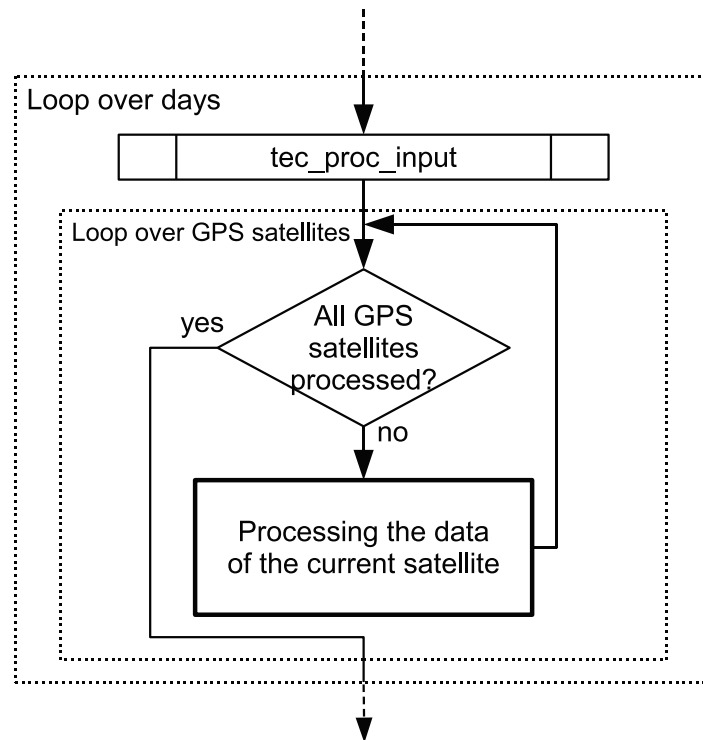
Figure 17: After all necessary data has been read in and prepared for analysis, a loop over the GPS satellites starts.

5.2.3. GPS data correction

Having the data of one satellite in continuous order, the first step inside the GPS satellite loop is the correction of the GPS data. The flow of the GPS data correction is illustrated in Fig. 18. There are four subroutines which are almost one-to-one adaptions of the routines from Stolle (2004). The cycle-slip detection in the wide-lane combination is implemented by the **tec_proc_wide_lane_detection** subroutine. To fit the detection to the data of the CHAMP POD antenna, a detection threshold of 2σ is chosen. As in Stolle (2004), outliers in the time series of the GPS observations ($N_{\delta\ i+1}$, see equation (26)) are interpolated with the relation $N_{\delta\ i+1} = 0.5(N_{\delta\ i} + N_{\delta\ i+2})$. After all observations of a GPS satellite have been analysed for cycle-slips, the data of the separated arcs are passed to the **tec_proc_polynom_n1_n2** subroutine.

This subroutine is used to test the connectivity of the separated arcs and to find the offsets ΔN_1 and ΔN_2 which are needed for the cycle-slip correction. The connectivity is tested with an extrapolation approach that has been fully inherited from Stolle (2004). Arcs with more

than 20 data samples are extrapolated using a cubic polynomial to the first 3 time stamps of the subsequent arc, arcs with more than 9 and less than 21 data samples are extrapolated with a quadratic polynomial, also to the first 3 time stamps of the subsequent arc, and arcs with less than 9 data samples are discarded due to uncertainties. The criteria for connectivity is given by the standard deviation of the difference between the extrapolated values and the original values of the to be connected arc. Two arcs are considered to be connectable if the standard deviation is less than 0.25. The necessary ΔL_I values (see equation (29)) to determine ΔN_1 and ΔN_2 are calculated as the difference of the first extrapolated sample of the first arc and the first original sample of the second arc.

The correction of the cycle-slips is divided into two subroutines, **tec_proc_carrier_shift** and **tec_proc_final_arcs**. In **tec_proc_carrier_shift** the ΔN_1 and ΔN_2 values from the preceding subroutine are used to correct the carrier phase observations after a cycle-slip to be aligned with the carrier phase observations before the cycle-slip. This step forms the basis for the creation of the finally phase connected arcs, which are created in **tec_proc_final_arcs**.
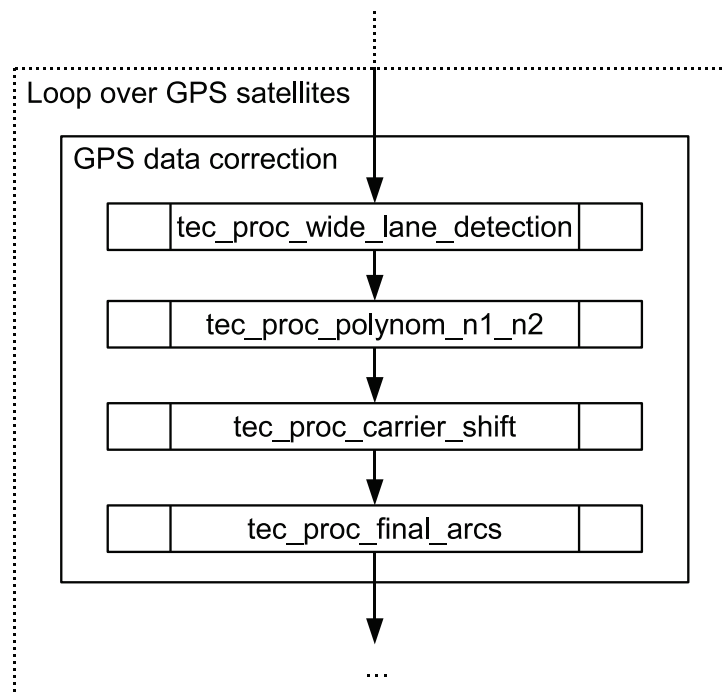
Figure 18: Implementation of GPS data correction

5.2.4. Multipath estimation

As stated in section 3.3, a weighted average of all P1 and P2 multipath combinations of a phase connected data arc is calculated to achieve a zero mean left-hand side of equations (31) and (32). The weighting is created by calculating the average of the signal-to-noise ratios of L1 and L2 for the arc. The multipath combination offsets B_{Pi} are calculated from observations that have at least the average signal-to-noise ratio. The P1 and P2 multipath values M_{Pi} are then calculated by subtracting the multipath combination offsets from the specific multipath combinations MC_{Pi} with:

$$M_{P1} = MC_{P1} - B_{P1}$$
$$M_{P2} = MC_{P2} - B_{P2}$$

(42)

To prevent outliers and to separate multipath from noise, the mean value of the multipaths with respect to the ray elevation and azimuth angles is calculated using a one degree grid similar to a histogram (see Fig. 19). The multipath values are fit into this grid by rounding the corresponding elevation and azimuth angles to the next integer. To calculate the multipath averages, the multipath values of the observations from all GPS satellites of a single day are needed. Therefore, the multipath estimation is calculated in the subroutine **tec_proc_multipath_calc** in its own loop over the GPS satellites before the actual TEC determination starts. As the data of only one satellite is stored at a time, the complete GPS data correction has to be calculated before **tec_proc_multipath_calc** is called for the multipath estimation (see Fig. 20).
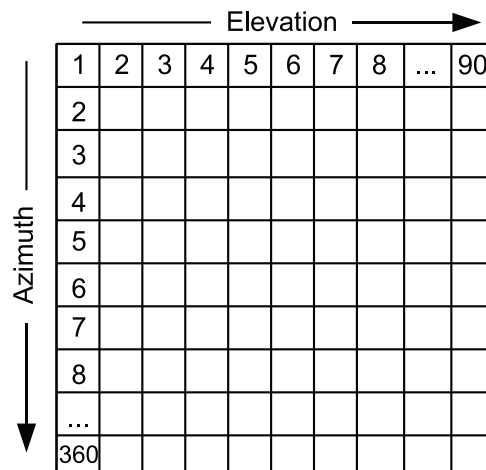
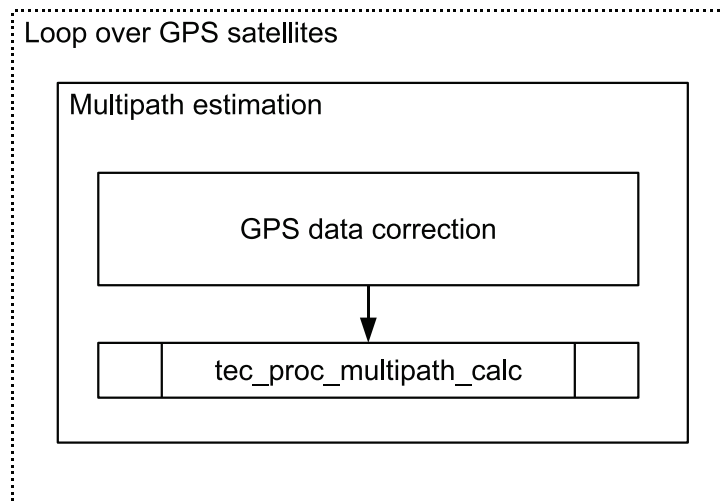Figure 19: Elevation-azimuth-grid for multipath averaging

Figure 20: Implementation of the multipath estimation

By default, the multipath values are only averaged from the data of the current day. This can be changed by the *multipath_average_all* configuration variable, which allows for a continuously calculated average over the complete period of time of the TEC processing. With the multipath estimation finished, the TEC determination is calculated in a new loop over the GPS satellites that starts with the GPS data correction and is followed by the correction of the code phase observations with the averaged multipath values, which is done in the **tec_proc_multipath_corr** subroutine. This step is referred to as "Multipath correction" in Fig. 14.

5.2.5. Resolution of the carrier phase ambiguities

After the code phase observations have been corrected for multipath, the carrier phase differences are shifted into to the code phase differences to resolve the carrier phase ambiguities. The corresponding subroutine is **tec_proc_code_shift**, which is also almost a one-to-one adaption of the routine from Stolle (2004). The shifting can be accomplished either by the mean value of the differences or the median value of the differences. The default shifting method is the mean value, but it can be changed with the *code_shift* configuration variable, which accepts *mean* or *median* as its value. The result of this subroutine are phase connected data arcs with low noise, non-ambiguous carrier phase observations which form the basis for the calculation of relative TEC.

5.2.6. Calculation of relative TEC

The subroutine **tec_proc_relative_tec** implements the calculation of relative TEC from the code-levelled carrier phase observations using equation (41). As the subsequent estimation of the receiver DCB is based on the analysis of simultaneous GPS observations, the data from the phase connected arcs of the separated GPS satellites are merged and ordered by GPS time. These merged data are also required for the text output of the TEC determination results. In addition to calculating relative TEC, the subroutine is also used to calculate the average RMS error between the TEC from the code phase observations and the TEC from the code-levelled carrier phase observations from all phase connected arcs to estimate the accuracy that has been achieved by the carrier-to-code-shifting algorithm.

5.2.7. Receiver differential code bias estimation

The receiver DCB estimation is implemented in **tec_proc_receiver_dcb** and starts by calculating a preliminary DCB value from all code-levelled carrier phase TEC values that have a corresponding ray elevation of at least $45°$. This elevation limit can be changed by the *dcb_elevation_limit* configuration variable. To prevent unstable results for the preliminary DCB value, a minimum of 50 TEC value pairs is required. Otherwise, the receiver DCB has to be extrapolated, which is described later in this section. The preliminary receiver DCB value and the corresponding satellite DCB value are then added to all carrier phase TEC values to check for negative TEC values in order to validate the result. If negative TEC values occur, the receiver DCB is increased by 0.1 TECU and the validation is repeated. As the carrier phase TEC values and satellite DCB values stay unchanged, the number of negative TEC values is reduced or remains constant when the receiver DCB is increased. The amount of negative TEC values that have been eliminated with every iteration step is the main termination criteria for determining the final value for the receiver DCB.

For terminating the iterative increase, the sequence of the last four iterations is analysed. The termination criteria is fulfilled if the amount of eliminated negative TEC values between the last four iteration steps is 4-3-2 or less and the lowest negative TEC value of the last iteration is less than -0.5 TECU. If the amount of negative TEC values has not declined in some iteration steps, for example in a 2-0-0 sequence, the receiver DCB value from the iteration step with the first occurrence of the least amount is chosen. To clarify the termination process, an illustration of two examples is depicted in Fig. 21. If the lowest negative TEC value in the last iteration step is greater than -0.5 TECU, then the iteration continues until no negative TEC values occur.

	Negative TEC values	Lowest negative TEC value	Receiver DCB	Satellite DCB
4	25	- 2.3 TECU	- 19.3 TECU	17.0 TECU
3	21	- 2.2 TECU	- 19.2 TECU	17.0 TECU
2	18	- 2.1 TECU	- 19.1 TECU	17.0 TECU
	16	- 2.0 TECU	**- 19.0 TECU**	17.0 TECU

	Negative TEC values	Lowest negative TEC value	Receiver DCB	Satellite DCB
2	22	- 2.1 TECU	- 20.6 TECU	18.5 TECU
0	20	- 2.0 TECU	**- 20.5 TECU**	18.5 TECU
0	20	- 1.9 TECU	- 20.4 TECU	18.5 TECU
	20	- 1.8 TECU	- 20.3 TECU	18.5 TECU

Figure 21: Receiver DCB iteration sequence termination

This distinction is applied to differentiate between outliers in the TEC values, which have to be left uncorrected for finding the target value of the receiver DCB and TEC values which are in the range of the receiver noise since a deviation of 0.5 TECU corresponds to a noise error of approximately 0.05 m.

The remaining number of negative TEC values at the end of the iteration is additionally used as a means of creating a quality index for the estimation of the receiver DCB. This quality index is implemented as a scale with five steps:

5   no negative TEC values

4   1 - 25 negative TEC values

3   26 - 50 negative TEC values

2   51 - 75 negative TEC values

1   76+ negative TEC values

With the iteration process terminated, the final receiver DCB value is by default calculated as the sliding average of the DCB values of the last three days in the TEC processing to smooth the value. The application of this sliding average calculation is determined by the *dcb_sliding_avg* configuration variable.

Although the described estimation method has proven to be robust, it cannot be excluded that there are days where the estimation method would create unstable results. Therefore, there is an additional fail-safe mechanism which is based on the receiver DCB average of the last 10 days. If the current DCB value deviates more than 3 TECU from the average, the receiver DCB value is extrapolated from the values of the last 5 days by a cubic spline. To have a properly adjusted average DCB value and to handle possible receiver DCB outliers at the beginning of the TEC processing which would cause all following valid DCB values to be recognized as outliers, the fail-safe mechanism does not take effect until at least 10 days have been processed. As the receiver DCB value is only calculated for days with valid input files, there can be large gaps in the sequence of the DCB values. To avoid unstable results, the extrapolation is applied only if the date of the last DCB value is not more than 5 days ago from the currently processed day. To indicate that the receiver DCB value was extrapolated, an additional sixth quality index value **0** is used.

Similar to the multipath estimation, the receiver DCB estimation requires the relative TEC values from the observations of all GPS satellites of a single day to create and solve the intended system of linear equations. Therefore, the receiver DCB estimation is calculated after the loop over the GPS satellites for the TEC determination has finished.

5.2.8. Output

After the receiver DCB value of the current day has been estimated, the results of the TEC determination are ready to be saved to a text file. Whether the output is created, is determined by the configuration variable *tec_output*. The text output of the automatic TEC processing is implemented in the **tec_proc_output** subroutine. As with the input files, there is a configuration variable named *tec_output_dir* to determine the directory for the output files and also an *output_by_year* configuration variable to specify whether there are sub-directories for different years. The name of the text output files is also generated by a pattern with `CH-POD-sTEC`**_year_** **doy**`.dat`.

As described in section 4.2.4, the main output file of the TEC determination results is a text list created on a daily basis. The file starts with a header section for the description of the content,
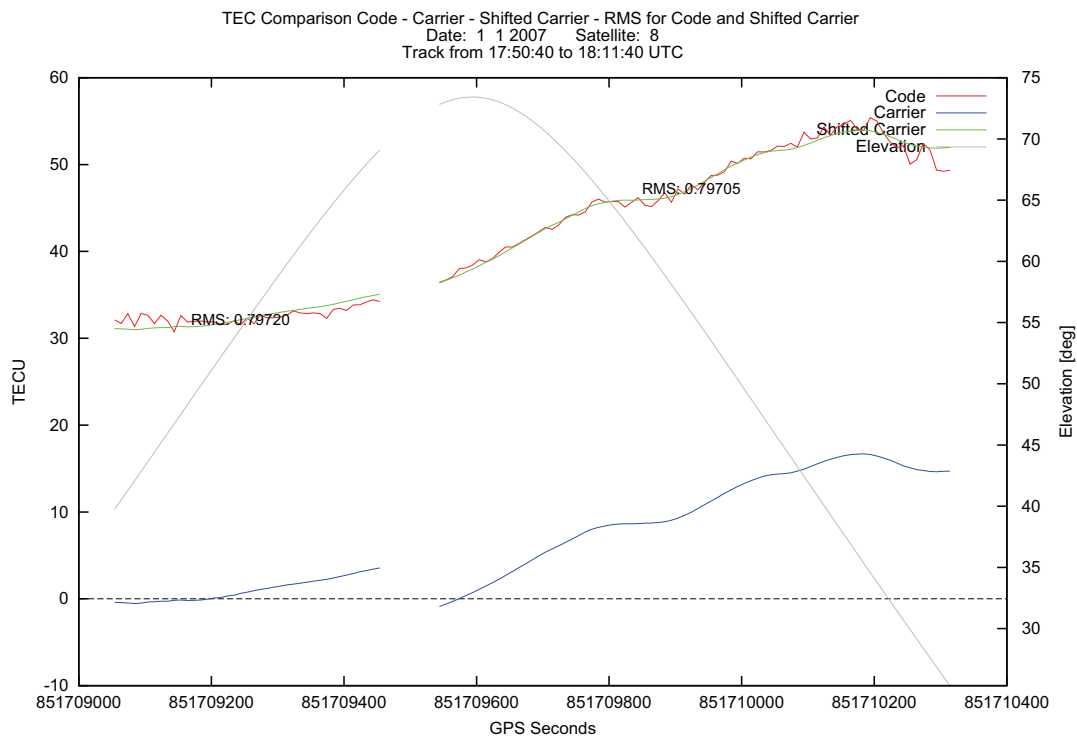
origin, and usage of the file, which is followed by the date of the processed day, the receiver DCB value of the day, and its quality index. As stated in section 4.2.3, it is not intended to provide absolute TEC values as the main result of the TEC processing, but the relative TEC values from the code-levelled carrier phase observations and the receiver DCB value. Subsequent to the receiver DCB value quality index, the results for each processed GPS observation are given. Similar to the input files, the results are ordered by GPS time. Besides the code-levelled carrier phase TEC value in the rightmost column, every observation in the list contains the GPS time stamp, the GPS satellite, the altitude of CHAMP, the X-,Y-,Z-coordinates of CHAMP and the GPS satellite in the WGS 84 reference frame, L1, L2, P1, P2, and the signal-to-noise ratios S1 and S2. An excerpt from a text output file is given in Fig. 22.

Figure 22: Example of text output

5.2.9. Graphical output with Gnuplot

As intended in section 4.2.4, the TEC processing program also offers the possibility of creating graphical output of the results using Gnuplot. There are three different plot types for the TEC results, the multipath results and the receiver DCB results. Each of these plot types requires the creation of a plot command file with information on how to create the plot and a data file containing the data to be plotted. Executing Gnuplot from the TEC processing program is accomplished by using the intrinsic subroutine *CALL SYSTEM*, which is intended to call external programs. In doing so, the plot command file is passed to Gnuplot.

Figure 23: TEC plot example

TEC plotting

The TEC results are plotted on a per-track basis of the GPS satellites. Due to uncorrectable cycle-slips and gaps in the time series, the data of one satellite track is often separated into several data arcs. To find all data arcs of one track, the time gap between the arcs is analysed. Arcs that are not more than 30 minutes apart are considered to belong to one satellite track. As there is a total number of approximately 300 to 400 tracks per day from all satellites, a multi-page Postscript plot is created containing the data of a whole day instead of a single plot for each track. A TEC plot contains TEC from the multipath corrected code phase differences, TEC from the carrier phase differences including the carrier phase ambiguities and TEC from the code-levelled carrier phases. Additionally, the RMS error between the code phase TEC and the code-levelled carrier phase TEC is given on a per-arc basis, as well as the elevation of the GPS observations during the satellite track. To identify each satellite track, the date and time, as well as the number of the satellite is given in the title of the plot. The time of the plotted TEC values is given in continuous GPS seconds starting January 6, 1980, 12 am. It has to be considered,

that all plotted TEC values are biased by the receiver and satellite DCB. An example of the TEC plot with an uncorrectable cycle-slip is given in Fig. 23.

The creation of the TEC plots is implemented in **tec_proc_tec_plotting**. This routine combines the two-step procedure of creating plots with Gnuplot. On the one hand it creates the necessary plot command file and the file containing the data to be plotted, which is referred to as "TEC plotting preparation" in Fig. 14. On the other hand it is used to call Gnuplot for the creation of the plot ("TEC plotting"). The plot command file and the data file are both continuously created during the loop over the GPS satellites for the TEC determination since the data of the phase connected arcs is only available for the currently processed GPS satellite. When the loop has finished, the subroutine is called a last time to create the plot. Whether TEC plots are created during the TEC processing is determined by the *tec_plotting* configuration variable, which is activated by default. The output directory of the TEC plots is determined by the *tec_plot_dir* variable in consideration of the *output_by_year* variable. The TEC plots are named by the pattern `CH-POD-sTEC`**_year_doy**`.ps`.

Multipath plotting

The results of the pseudo-range multipath estimation are plotted in the form of a sky plot (see Fig. 24). The position of the multipath value is presented in polar coordinates where the azimuth angle of the GPS observations with respect to the flight direction of the CHAMP satellite is indicated by the circular angle of the plot and the elevation angle of the observations is specified by the radius from the boundary to the center of the circle. Following the approach from Montenbruck and Kroes (2003), the magnitude of the multipath values is indicated by a color map on a scale between -3 and 3 metres.

The corresponding plotting subroutine is **tec_proc_multipath_plotting**, which also combines the preparation and the creation of the multipath plots. The multipath plots are also created after the loop over the GPS satellites for the TEC determination has finished. The output directory of the multipath plots is determined by the *multipath_plot_dir* variable. The naming pattern is `CH-POD-MP1`**_year_doy**`.ps` and `CH-POD-MP2`**_year_doy**`.ps`, respectively. To create these plots, each averaged multipath value has to be plotted separately, which causes a considerably longer plotting time in comparison to the other plot types. Therefore, the multipath plotting is deactivated by default during the TEC processing. Whether the multipath plots are created can be set with the *multipath_plotting* configuration variable.
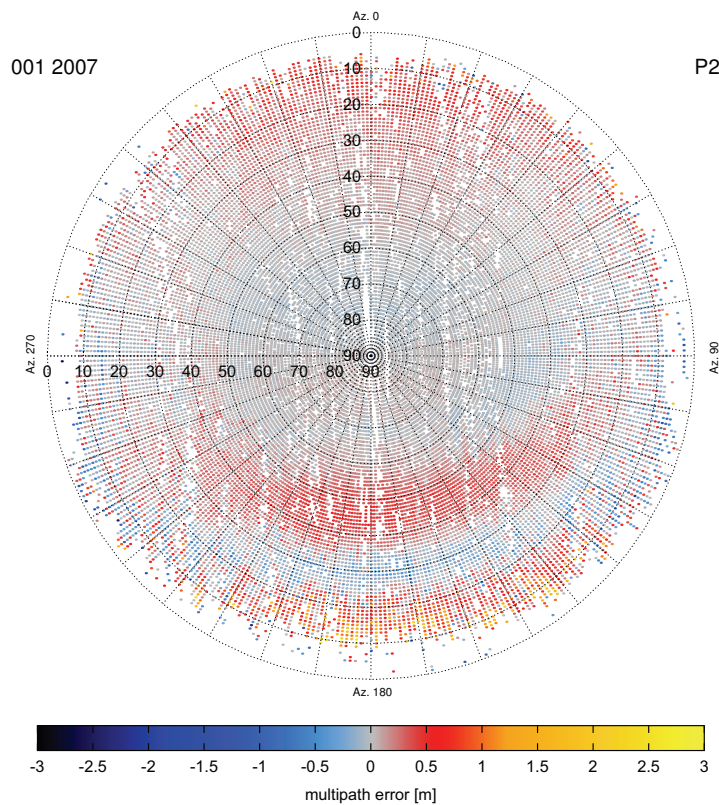
Figure 24: Multipath plot example

Receiver differential code bias plotting

The plot that is created at last is the receiver DCB plot. As there is only one DCB value per day, the values of the whole TEC processing time period are plotted into one Postscript file. An example for a receiver DCB plot is given in Fig. 25. Besides the DCB values, the plot also illustrates the number of TEC value pairs that has been used for the first approximation of the DCB and the number of remaining negative TEC values at the end of the DCB iteration. To have a continuous date format that allows for a non-ambiguous determination of the DCB values in multi-year plots, the date of the DCB values is given in Modified Julian Day (MJD) starting at January 1, 2000, 12 am. The plotting subroutine for the receiver DCB is **tec_proc_dcb_plotting**. Like the other two plot subroutines, it implements the plotting preparation and the plotting itself. The plotting preparation is done in the loop over the days after the estimation of the receiver DCB has finished and the plot is created after all days have been processed. The creation of the receiver DCB plot is activated or deactivated by the *dcb_plotting* configuration variable.
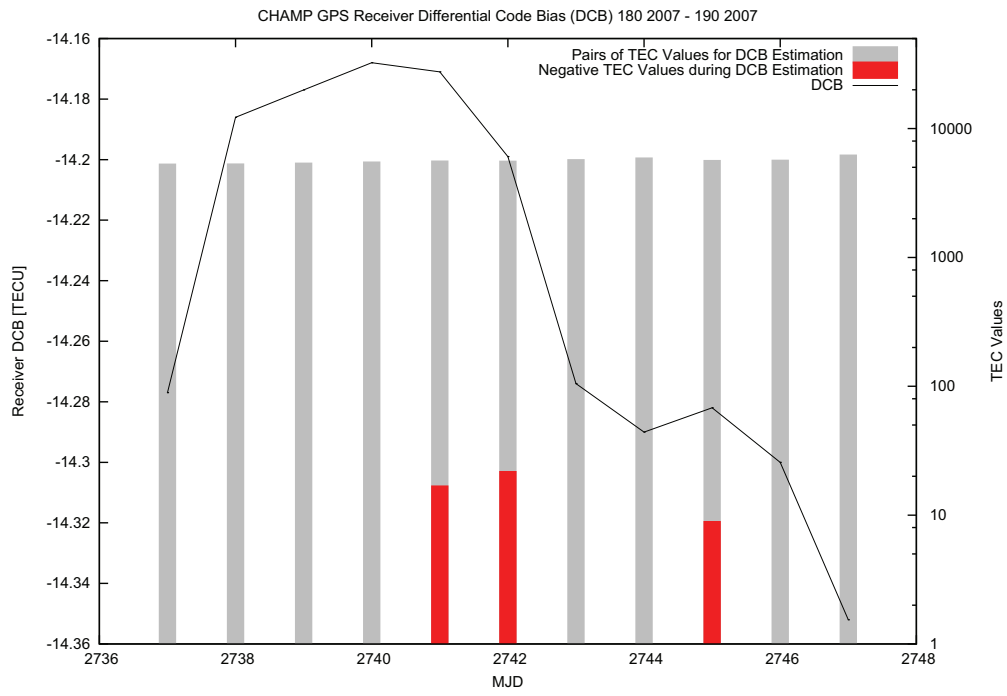
Figure 25: Receiver DCB plot example

6. Results and discussion

This section presents and discusses the results that have been achieved with the implementation of the automated TEC determination. The TEC processing was applied between day 1 2001 and day 365 2009. Since the processing of all data was completely free of errors, the implementation can be assumed to work stable. Although all parts of the implementation have been thoroughly tested, undetected errors in the program cannot be excluded entirely. At first, the results of pseudo-range multipath estimation are presented since they have a significant influence on the results of the receiver differential code bias estimation and the TEC results, which are described afterwards.

6.1. Multipath

The results of the multipath estimation have to be separated into three different periods of time due to modified GPS receiver and antenna configurations. The first and longest period is from day 1 2001 to day 278 2008 where the occultation antenna and the pre-amplifier of this antenna were active and the main GPS receiver was used. The second period is from day 288 2008 to day 308 2008. On day 288 2008 the occulation antenna was deactivated and additionally the spare GPS receiver was used henceforward. However, the pre-amplifier of the occultation antenna was still active and not deactivated until day 309 2008. This creates the third period of time from day 309 2008 to day 365 2009.

An example of the results of the first period is given in Fig. 26 with the P1 and P2 multipath values on day 180 2007. The P1 multipath mostly varies between approximately -2 m and 0.6 m. The multipath on P2 is generally higher with values up to 3 m. The most noticeable property of both plots is an oscillation at the rear side of the antenna (90° to 270° azimuth) causing the largest multipath values. These oscillations are also stronger on P2 than on P1. To analyse the occurrence of these oscillations, the average multipath over the whole year 2007 has been calculated, which is depicted in Fig. 27. The plots show that the oscillations are not a time-dependant disturbance. Oscillations also occurred on all other days in the first period where the occultation antenna and its pre-amplifier were active. Since the occurrence is completely confined to the rear side of the POD antenna, the origin of these strong multipath values is probably located at the aft-panel of the CHAMP satellite.

An example of the multipath results for the second period is depicted in Fig 28. The plots illustrate almost the same multipath distribution and magnitude as in the first period. Oscillations at the rear side are also present and not time dependant as well. In contrast to the first period,

there are larger gaps in the multipath values which are mostly confined to the front side of the POD antenna. The increased gaps are due to the lesser amount of GPS satellites the spare GPS receiver is able to track. A reason for the confinement to the front side of the antenna cannot be given however.

Looking at a result of the third period in Fig. 29, the oscillations have completely vanished, which is also the case for all other days in that period. Since the only difference to the second period is the deactivation of the pre-amplifier of the occultation antenna, this pre-amplifier can be determined as the cause of the oscillations. A similar multipath distribution is given for the main GPS receiver on day 310 2002 (see Fig. 30), which is the only day in the first period with an inactive occultation antenna and pre-amplifier. Without oscillations, the plots illustrate an almost linear increase of the multipath errors from high to low elevations. Additionally, the magnitude of the multipath on P1 and P2 appears to be almost equal. Even without oscillations, the multipath below an elevation of 20 degrees tends to be quite strong and also unstable in certain cases.

In the implementation of the TEC processing the attitude deviations of the CHAMP satellite were omitted during the calculation of the elevation and azimuth angles for reasons of simplicity and execution speed. As the attitude of the CHAMP satellite is very stable, the deviations reach a maximum of two degrees in all directions, which is negligible for most applications. However, with these strong multipath oscillations occurring most of the time in the CHAMP GPS observations, the effect of a deviation correction on the multipath results was additionally investigated. The necessary attitude deviations were provided by Department 1.2 of the GFZ in the form of roll, pitch, and yaw angles for the year 2008. To visualize the effect of the attitude correction, the absolute difference between corrected and uncorrected multipath values is depicted in Fig. 31 for day 10 2008. It can be seen that considerable differences mostly appear in elevation regions below 25 degrees and regions of multipath oscillations.

In perspective of the Swarm satellite mission, strong multipath oscillations are not expected due to missing occultation devices of the satellites. However, the attitude of the Swarm satellites might not be as stable as CHAMP's. Therefore, a correction of the satellite attitude is very favourable to estimate the multipath errors as exact as possible.
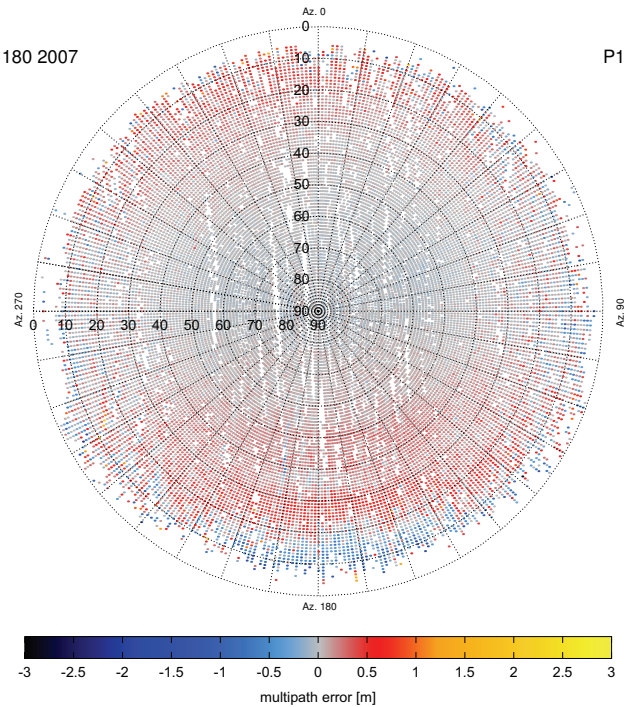
(a) P1 multipath estimation
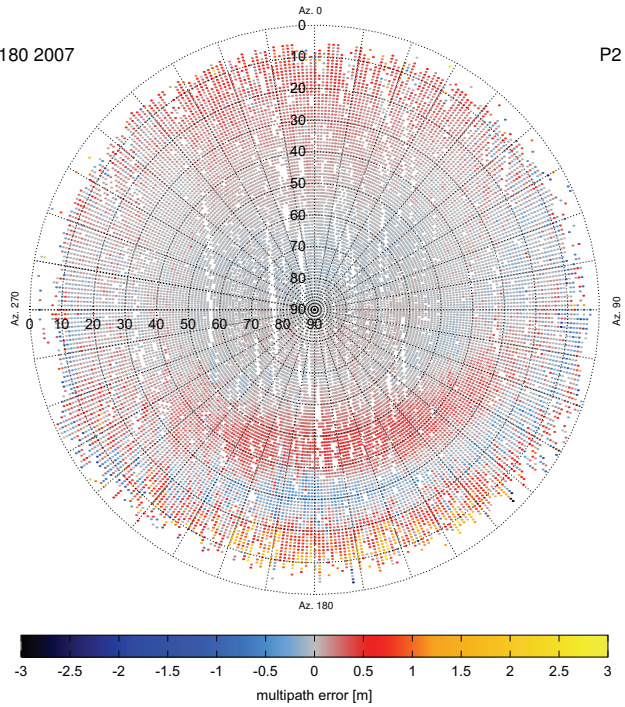
(b) P2 multipath estimation

Figure 26: Multipath estimation for day 180 2007
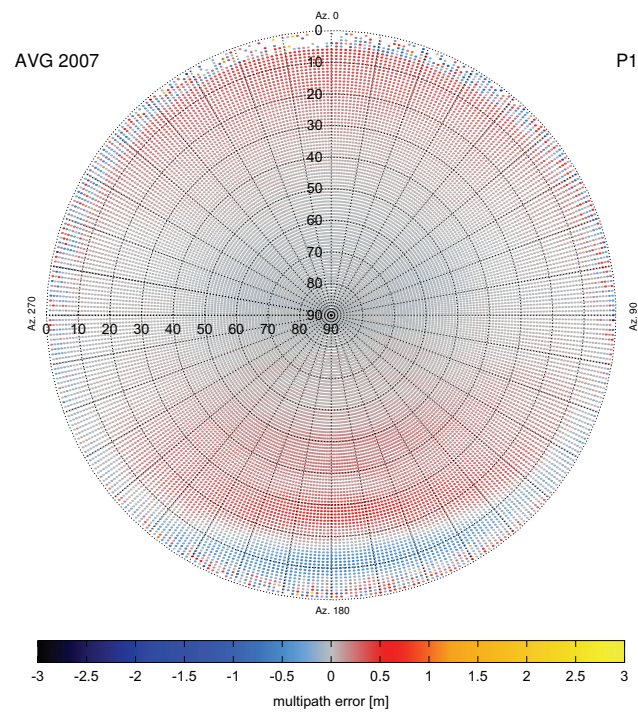
(a) P1 multipath estimation
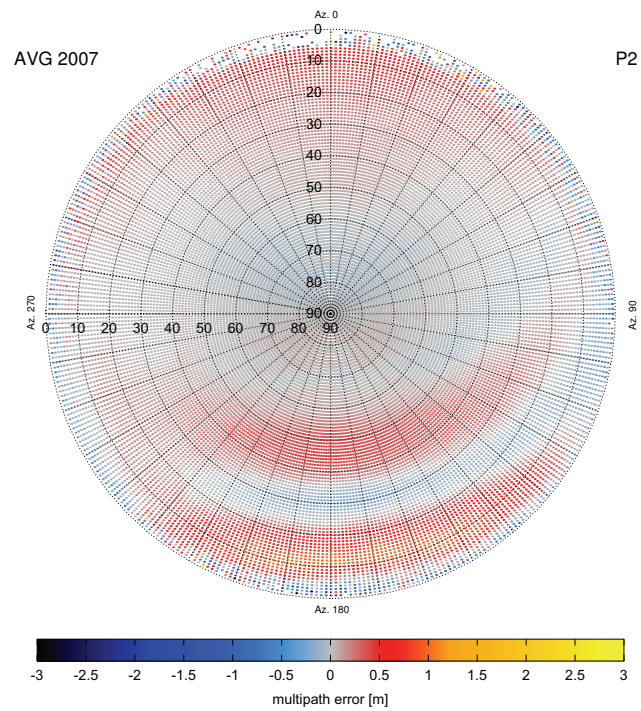
(b) P2 multipath estimation

Figure 27: Average multipath for the year 2007
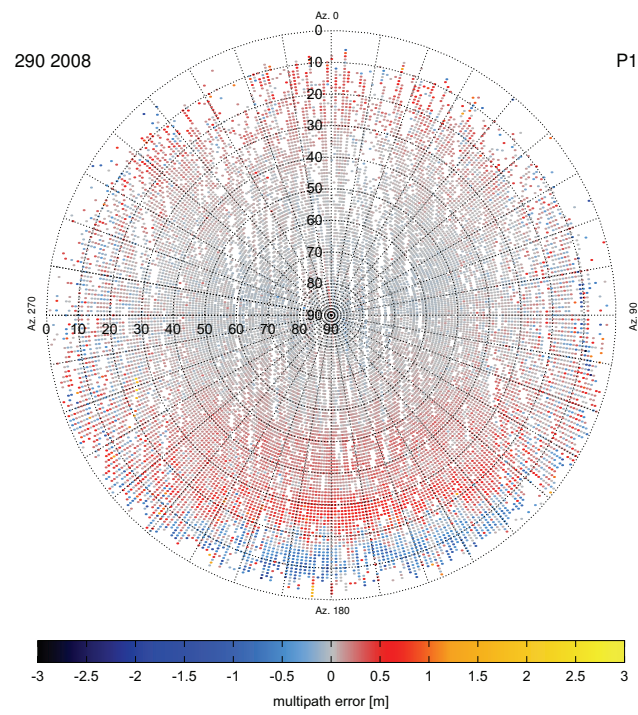
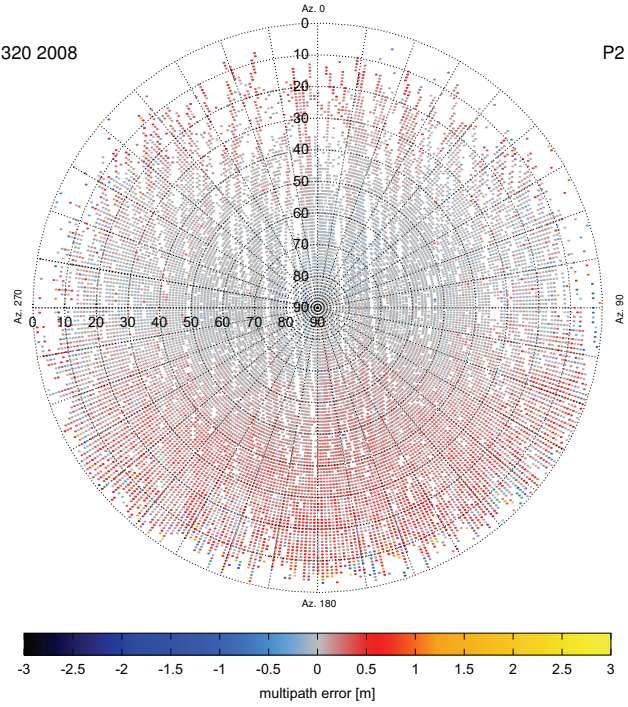(a) P1 multipath estimation
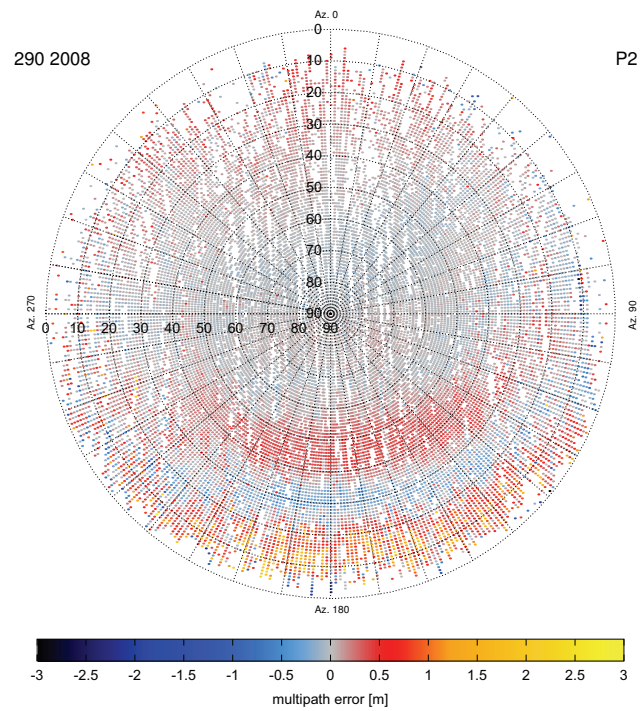
(b) P2 multipath estimation

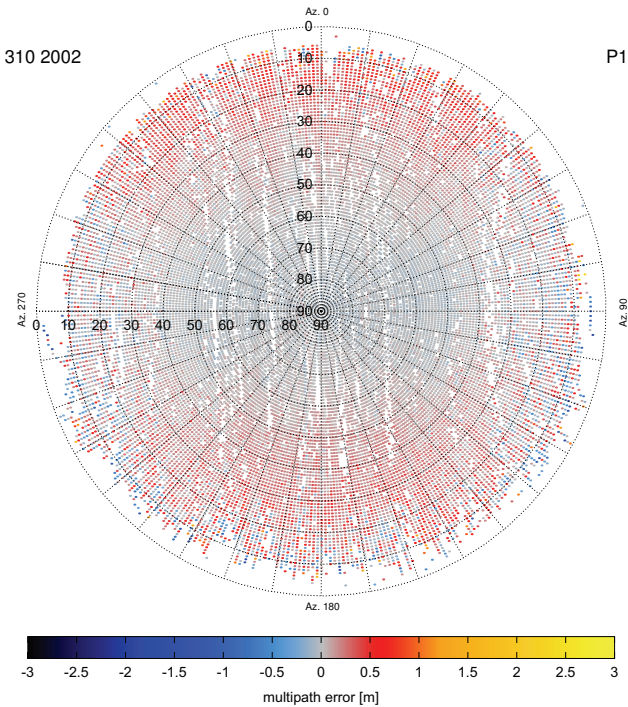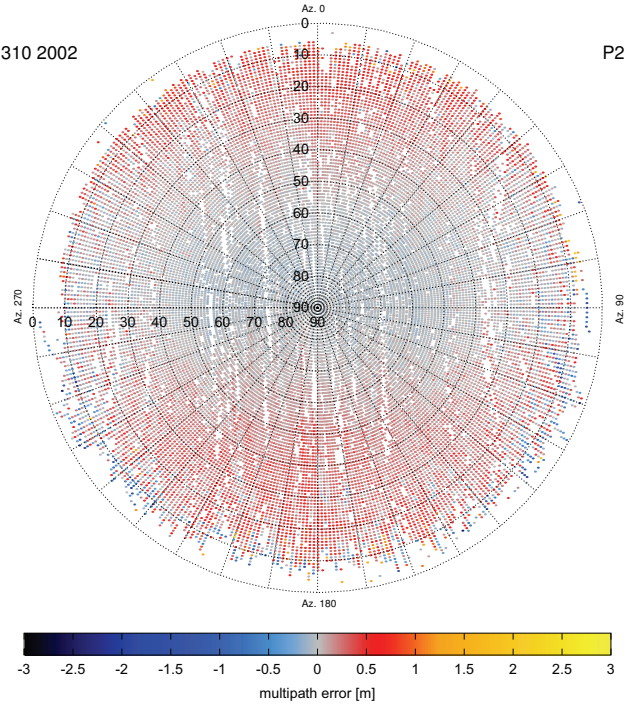Figure 28: Multipath estimation for day 290 2008
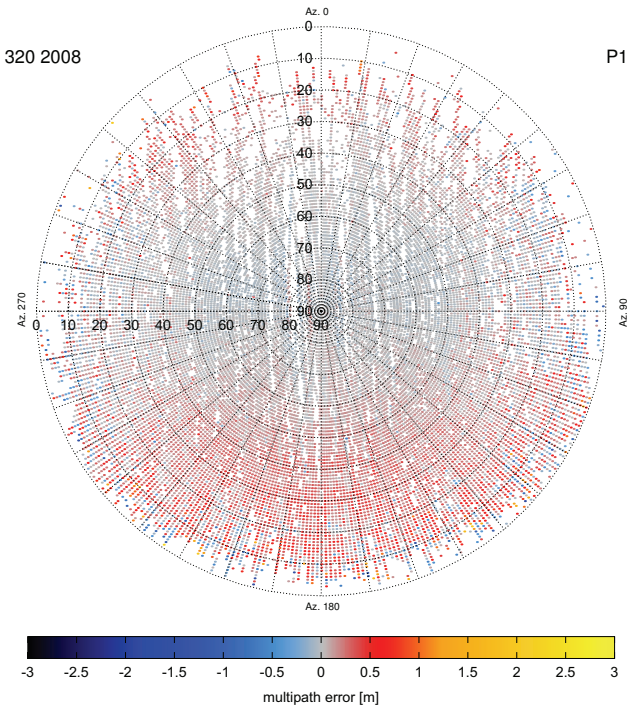
(a) P1 multipath estimation

(b) P2 multipath estimation
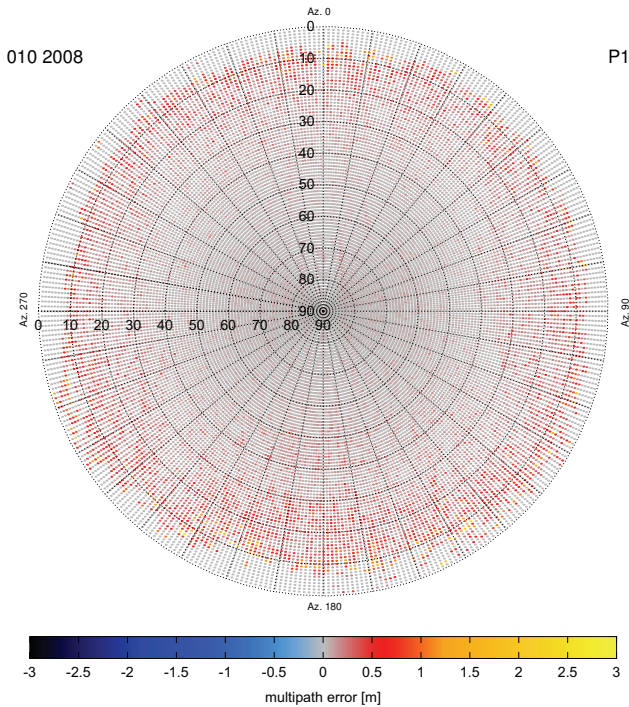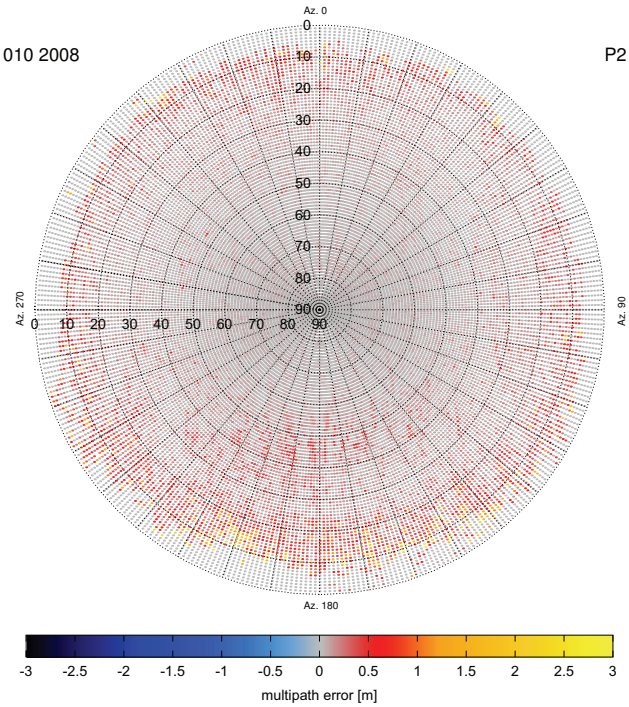
Figure 29: Multipath estimation for day 320 2008

(a) P1 multipath estimation

(b) P2 multipath estimation

Figure 30: Multipath estimation for day 310 2002

(a) P1 multipath correction difference

(b) P2 multipath correction difference

Figure 31: Multipath attitude correction difference for day 10 2008

6.2. Receiver differential code bias

Due to the multipath errors in low elevations, the results of the receiver DCB estimation and the TEC determination are based on a processing with a minimum elevation limit of 25 degrees for all input data. A detailed explanation for this decision has been given in section 6.1. A plot of the results from day 1 2001 to day 365 2009 is given in Fig. 32. The vertical dashed line denotes the change of the GPS receiver. The average receiver DCB for the complete period is approximately -16.5 TECU, reaching from -25 TECU in 2002 to -12 TECU in 2009. The RMS error for the day-to-day variation of the DCB is 0.2 TECU with sliding average calculation and 0.9 TECU without averaging, hence a stable solution is achieved. From 2857 processed days, 578 had remaining negative TEC values at the end of the DCB iteration process with an average of 28.4 negative TEC values per day, which corresponds to an outlier rate of less than one percent, assuming an average amount of 40,000 to 50,000 TEC values per day. The receiver DCB had to be extrapolated for 13 of the 2857 processed days, which is also less than one percent. Based on the achieved results, the iteration approach for the receiver DCB estimation can be assumed to be robust.
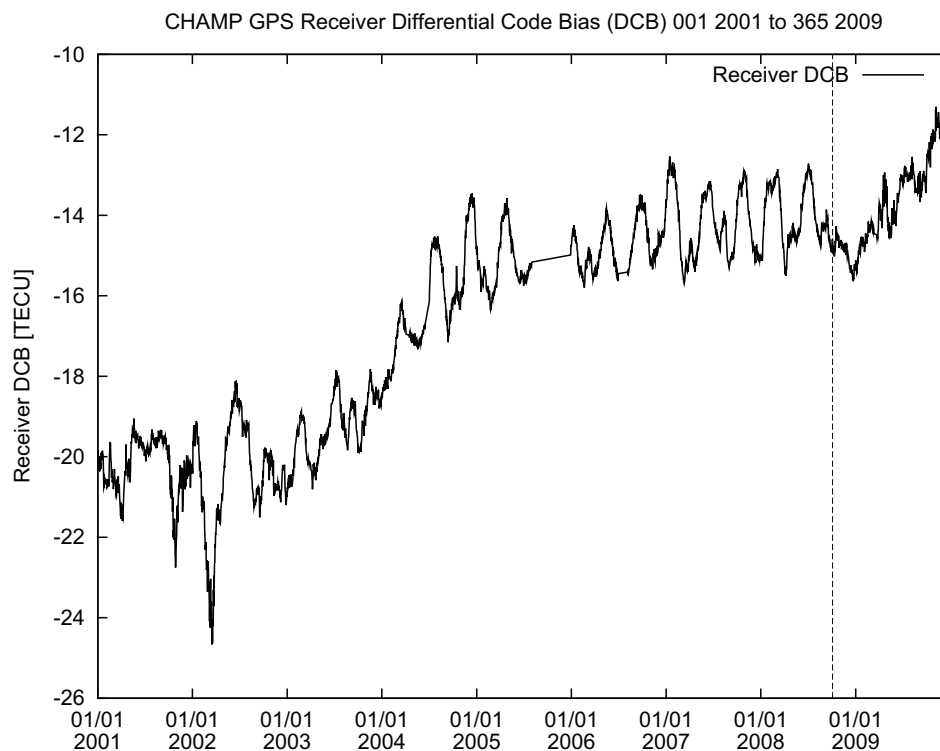
Figure 32: Receiver DCB results for 2001 to 2009
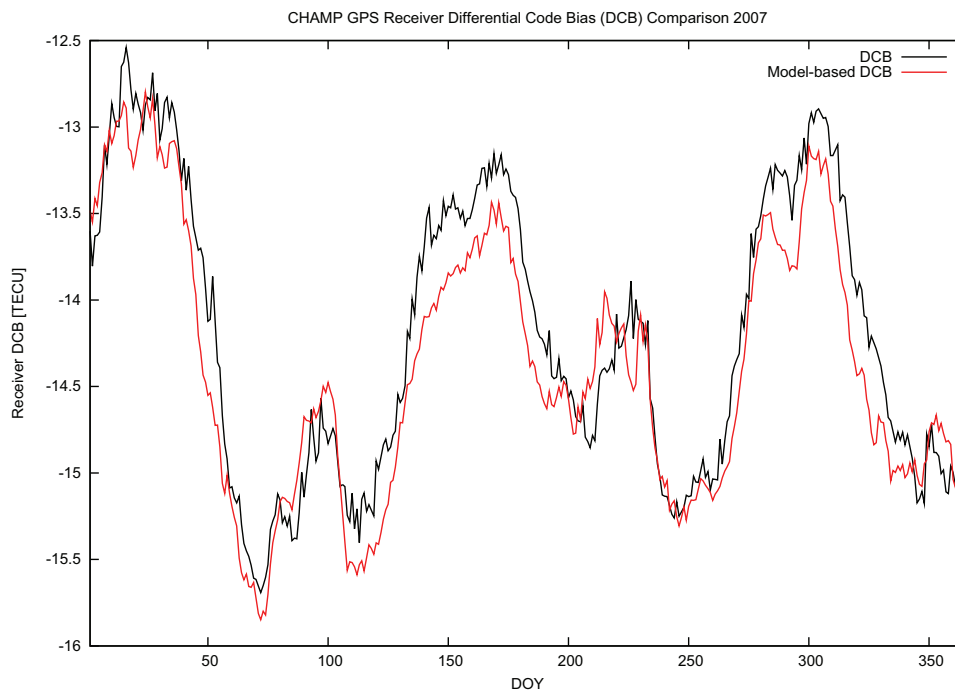
Figure 33: Receiver DCB comparison for 2007

The following analysis of the receiver DCB results is focussed on the year 2007 since addi-
tional data was available for this period of time to compare, validate, and interpreted the results.
For comparison and validation, the receiver DCB results of 2007 are plotted with the receiver
DCB values of the model-based approach from Heise et al. (2003), which is depicted in Fig. 33.
The magnitude and trends of the receiver DCB values are very similar. Differences occur espe-
cially in the minima and maxima regions of the receiver DCB. These recurring variations in the
DCB values can also be seen in Fig. 32 and have been further analysed.

As mentioned before, the DCB is an error caused by the receiver hardware, which is sub-
ject to external influences such as solar radiation. Since the CHAMP satellite is not on a sun-
synchronous orbit, the varying local time of the CHAMP satellite at equator crossings has been
compared to the receiver DCB results. This comparison is illustrated in Fig. 34. It can be seen
that the receiver DCB maxima always occur approximately at 12 am/pm (red vertical lines),
whereas the local maxima in the minima regions always occur around 6 pm/am (blue vertical
lines). These results led to the assumption of a temperature dependence of the receiver DCB.
To verify this, the CPU temperature of the CHAMP satellite was compared to the receiver DCB
values, which is illustrated in Fig. 35. The plot clearly indicates a variability of the receiver
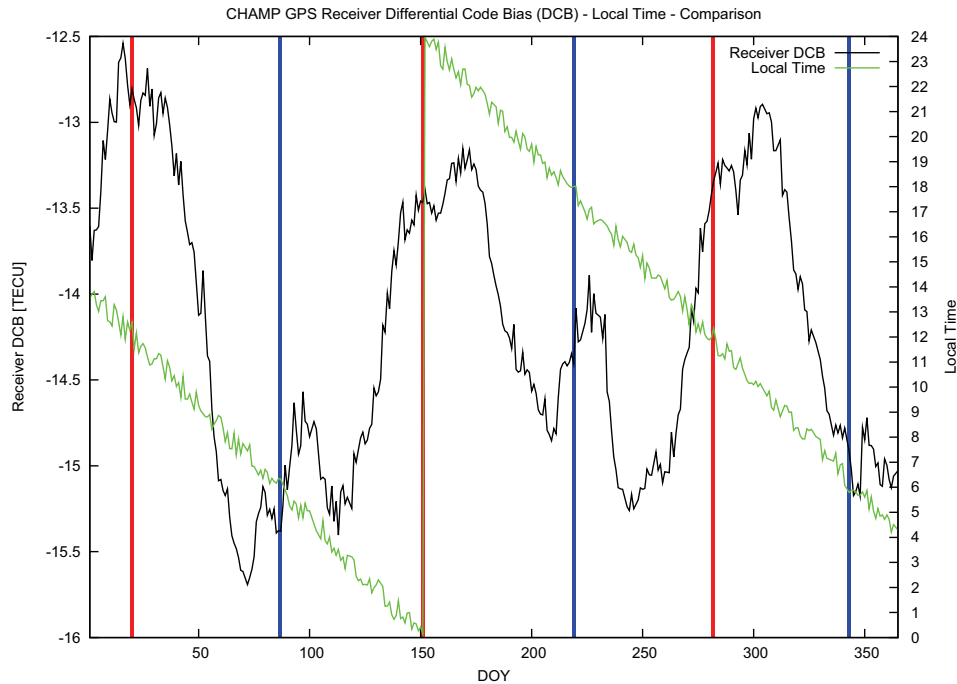
Figure 34: Receiver DCB and local time for 2007

DCB with respect to the temperature, although a linear correlation is not given. The most noticeable property of the temperature dependence is a very high sensitivity of the receiver DCB to temperature enhancements in 6 am/pm orbits and a comparatively low sensitivity in 12 am/pm orbits. A reason for this behaviour of the receiver DCB has not been found. It has to be considered, however, that it is not a comparison to the temperature of the GPS receiver, which was not available.

Due to the temperature dependence of the receiver DCB, the influence of solar activity has been analysed. In doing so, the solar radio flux index, also known as F10.7 index, which is a good indicator of solar activity, has been compared to the receiver DCB results of the complete processing period. This comparison is depicted in Fig. 36. Starting with approximately -21 TECU in 2001, the receiver DCB constantly increased, except for small recurring variations and some stronger deviations at the beginning of 2002, to approximately -14 TECU in 2006. Afterwards, the receiver DCB almost remained at that level until the GPS receiver changed. The results of the period with the spare GPS receiver are not comparable to the preceding results due to the significantly reduced amount of GPS observations. The solar flux index in turn almost constantly decreased until 2006 and remained very stable afterwards. This trend corresponds inversely to the receiver DCB and confirms the assumption of a general temperature dependence.
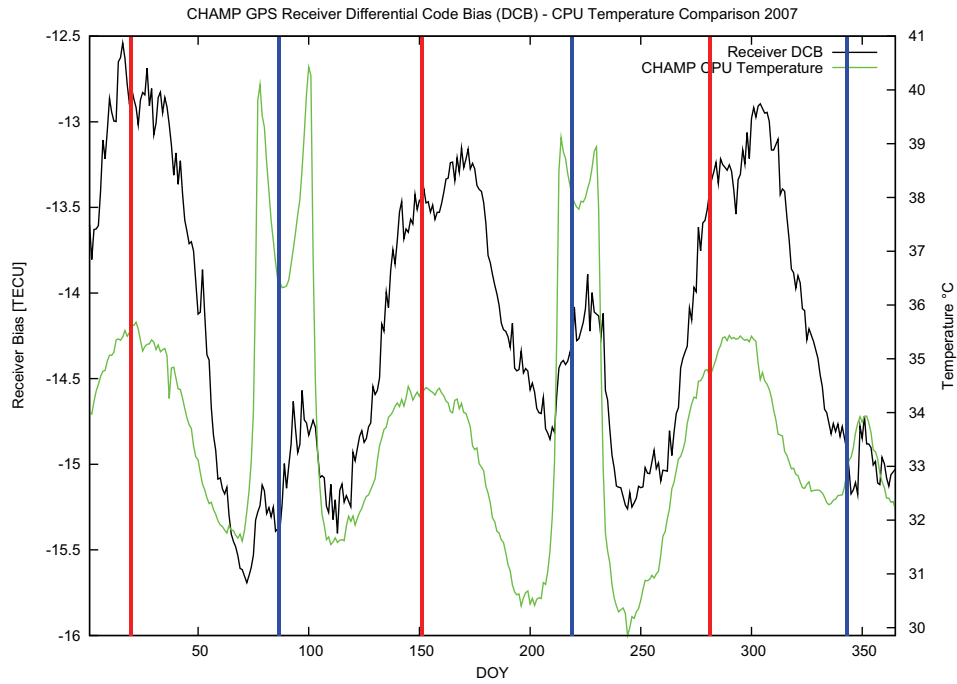
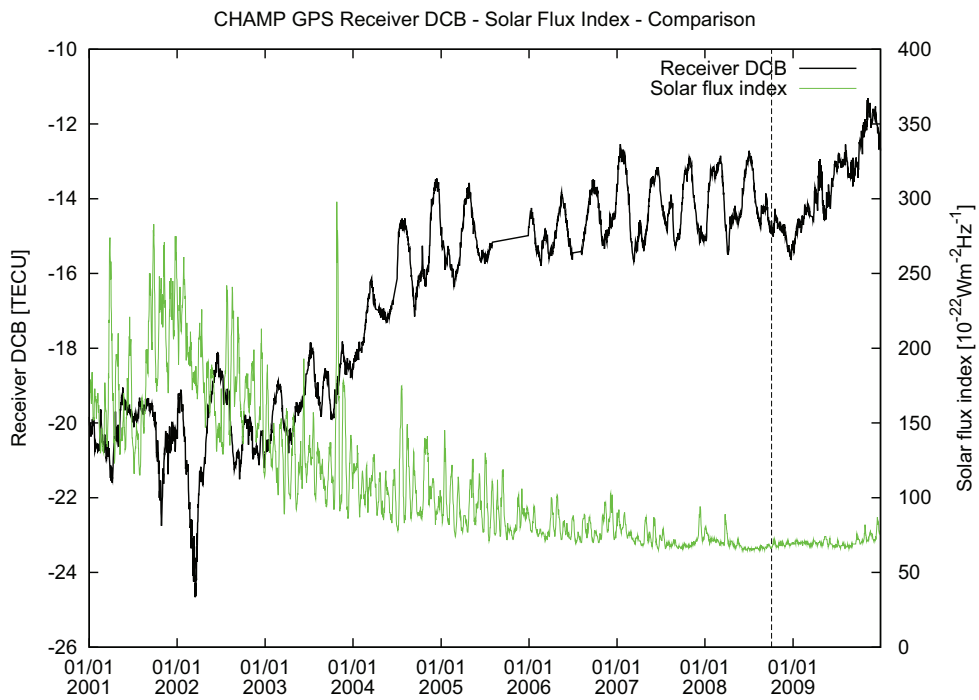Figure 35: Receiver DCB and CPU temperature for 2007

Figure 36: Receiver DCB for the complete TEC processing time period and solar flux index

6.3. TEC

The results of the TEC determination show typical ionospheric TEC values from 0 to 100 TECU for the majority of days in the processed period. There are also days with high solar activity, especially in 2001 and 2002, where TEC values reach magnitudes up to 200 TECU. Like the receiver DCB, the ionospheric TEC results show a correlation with solar activity. A comparison of the daily average TEC and the solar flux index is given in Fig. 37, which presents similar trends. However, a strictly linear correlation is not given.

The accuracy of the achieved TEC results is given by the average RMS error between the code-levelled carrier phase TEC and the code phase TEC. Thereby, an additional distinction between multipath corrected and uncorrected code phase TEC values has been made. The average RMS error for the entire processing period with uncorrected multipath is approximately 1.5 TECU and improves to 1.2 TECU with the multipath correction applied. To illustrate the impact of the multipath, an example plot with uncorrected and corrected code phase TEC values is given in Fig. 38. The plot also illustrates that the multipath estimation mostly succeeded in removing the oscillations on the rear side of the POD antenna while preserving the small scale noise error in high elevations.
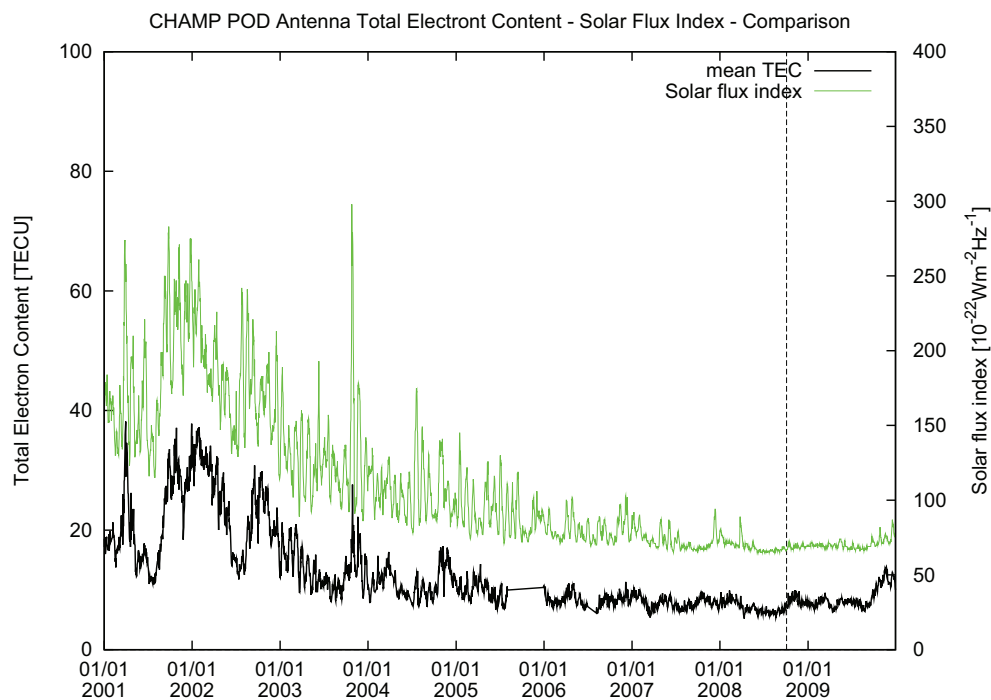
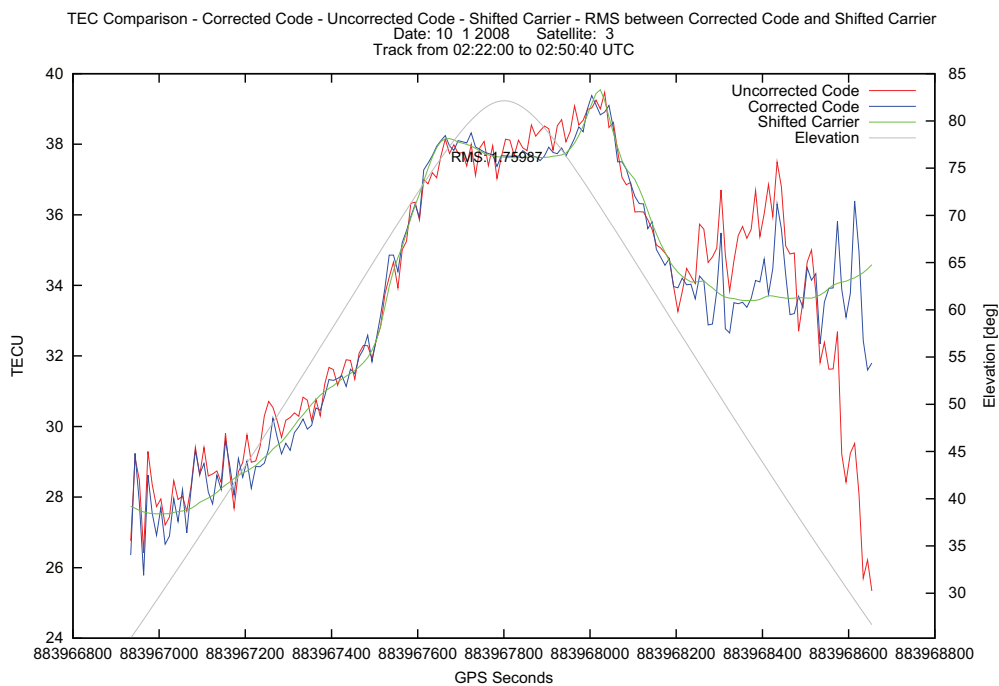Figure 37: Mean TEC long-term trend and solar flux index

Figure 38: Influence of multipath correction on the TEC determination

6.4. Limitations

The implemented TEC determination approach allows for the automatic creation of stable results on a daily basis, but there are also certain aspects of the implementation and external conditions which limit the functionality of the TEC determination program.

In general, the most limiting factor in retrieving TEC successfully, is the quality and amount of input data that can be analysed by the TEC determination program. This especially holds for the algorithms to estimate the receiver DCB and multipath, which rely on an adequate amount of data to work properly. Another limiting factor that applies for processing CHAMP data are the multipath oscillations on the rear side of the POD antenna. These disturbances effect the complete TEC processing beginning with the correction of the GPS observations. The utilized cycle-slip detection algorithm regularly detects a false cycle-slip between 15 and 25 degrees on the rear side of the antenna due to an abrupt change in the code phase data that was caused by multipath. This problem could not be fixed by changing the detection parameters since the algorithm is not designed to overcome this kind of error. Due to these falsely detected cycle-slips, isolated low elevation arcs with very strong multipath errors are created (see Fig. 39). As
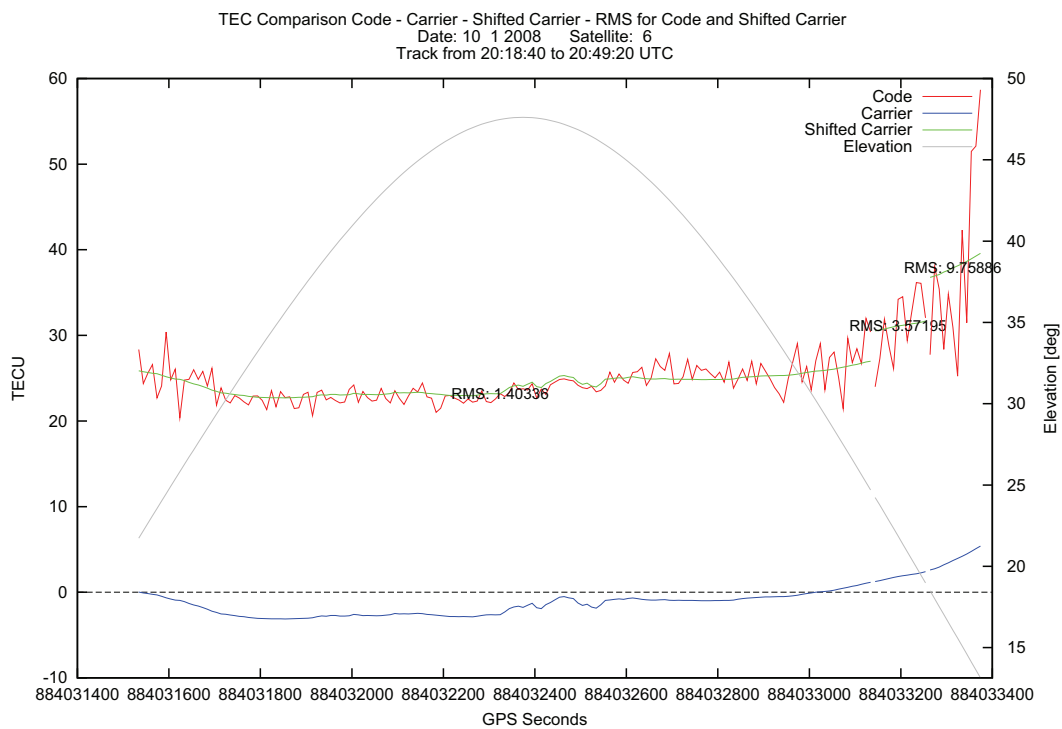
Figure 39: TEC determination with low elevation data

can be seen in the plot, the multipath of these arcs can hardly be corrected, hence the possibilities of resolving the carrier phase ambiguities properly are strongly degraded. This in turn effects the TEC determination and the estimation of the receiver DCB. Therefore, the critical elevation of 25 degrees was chosen as the default input elevation limit for the TEC determination from CHAMP data.

The implementation of the TEC processing routines is limited to some extent by the absence of dynamic memory allocation in Fortran 77. The number of days that can be analysed at one execution is for example limited to 5000. This limitation of preset dimensions also holds for other parts of the implementation so that certain dimensions in the TEC processing implementation have to be adapted if the amount of data exceeds the existing limits. Since the limits have to include a certain tolerance, preset and fixed dimensions also cause a waste of memory in many cases. Another limitation relates to the implementation of the receiver DCB estimation which relies on available results from preceding days to enable a sliding average calculation and a possible extrapolation. Therefore, a single-day processing is not recommended as it contains the risk of creating an unstable DCB value.

6.5. Performance analysis

This section presents an analysis of the performance that is achieved by the TEC determination program. The analysis is based on a test system with a 64 bit Ubuntu 10.04 operation system running on a PC with an AMD Athlon 64 X2 4600+ processor (2.4 GHz) and 4 GB of RAM. For the performance analysis, the TEC determination program was compiled using the gfortran compiler because the g77 compiler has an error in the system clock function, which is required to measure the execution time inside the Fortran routines.

At first, the pure processing time was analysed, hence all output was disabled. To estimate the influence of the data amount, four different input elevation limits were used. As a reference, day 180 2007 was used for the analysis since it provides typical values in terms of data amount, data characteristics, and results. The results of this analysis are calculated as the average value of 10 measurements and are given in Table 1. It can be seen that the processing time decreases with the amount of data that has to be processed. However, the correlation is not linear, which is probably due to the non-linear distribution of the data in respect of the elevation. Following the pure TEC determination calculations, the processing time depending on the output was analysed. Based on a default configuration which includes a disabled debug mode, an input elevation limit of 25 degrees, a receiver DCB elevation limit of 45 degrees, and enabled text output, the analysis has been done for five different output configurations for day 180 2007. The first configuration contains no plotting, the second configuration contains only TEC plotting, the third configurations contains only receiver DCB plotting, the fourth configuration contains only multipath plotting, and the fifth configuration contains all types of plots. The results of this analysis are also the average of 10 measurements and can be found in Table 2.

The configuration without any plotting, which is intended to be used in practise, achieves a stable processing time of approximately 7 seconds per day. Hence, a near real-time calculation of TEC is accomplished. The multipath plotting causes the largest increase in processing time with approximately 25 seconds, which is due to the fact that each of the up to 32400 multipath values has to be plotted separately to create this plot type with Gnuplot. The TEC plotting increases the processing time only by approximately 5 seconds. The additional time for TEC plotting strongly depends on the amount of data that is processed as well as the amount of satellite tracks since each track is plotted separately. The increase due to the receiver DCB plotting of a single day is negligible. The application of the receiver DCB plotting is generally intended for longer processing periods. Creating the complete output results in a processing time that is below one minute, which is still included in near real-time understanding.

Elevation limit	0°	15°	25°	45°
Time [s]	5.31	4.98	4.35	3.97

Table 1: Performance analysis for TEC processing without output

Plot type	None	TEC	Receiver DCB	Multipath	All
Time [s]	7.13	12.26	7.15	32.23	37.55

Table 2: Performance analysis for TEC processing with output

Besides the creation of graphical output, the TEC determination program has another performance drawback which cannot be disabled. The decision to store the data of only one GPS satellite during the TEC processing causes the need to recalculate several processing steps. To estimate the effect of the recalculations on the processing time, the TEC determination program was experimentally rewritten to store the data of all GPS satellites and omit recalculations. The general processing time of a day decreased by approximately 0.5 seconds. However, the memory consumption of the program increased from approximately 89 megabytes to 870 megabytes. Although modern PCs generally offer an adequate amount of RAM, the speed gain was neglected in favour of a moderate memory consumption.

7. Conclusion and outlook

This work describes a procedure to automatically retrieve ionospheric and plasmaspheric TEC from space-based GPS observations based on data of the POD antenna aboard the CHAMP satellite. The main part of this work consists of the adaption and integration of existing TEC determination routines into an automatic processing algorithm with the addition of an integrated estimation of pseudo-range multipath and the differential code bias of the TRSR-2 GPS receiver aboard CHAMP. The outcome of this work and important conclusions are described in the following:

- The TEC retrieval program is a user-friendly and highly configurable command-line application that enables a stable operation with reliable ionospheric TEC results on a routine basis. The results of the TEC retrieval are stored in a plain text file created on a daily basis, which is convenient for further use. Besides TEC results with auxiliary information, the text file contains the receiver DCB value of the day with an evaluating quality index. For evaluation and validation of the achieved results, the TEC retrieval program optionally offers the creation of graphical output. The TEC determination program additionally achieves a near real-time retrieval of TEC, which was one of the main objectives of the implementation.

- The integrated pseudo-range multipath estimation succeeds in correcting the majority of P-code observations. There are, however, limitations in correcting multipath anomalies caused by the CHAMP GPS antenna-receiver configuration. The occurrence of these multipath anomalies has been shown in Montenbruck and Kroes (2003) for CHAMP data of 2001 and 2002, and has now been further investigated for all available CHAMP data until the end of 2009. This investigation confirms an interference of the pre-amplifier of the CHAMP occultation antenna causing large multipath oscillations at the rear-side of the POD antenna.

- The included receiver differential code bias estimation, which is a new implementation of the method described in Syndergaard (2007) with an additional iteration approach to exclude outliers, achieves stable results and a moderate long-term trend with low day-to-day variations which were validated by independent comparison data. A further investigation of the receiver DCB showed recurring temperature dependent variations and an inverse correlation with the solar radio flux (F10.7) index.

In view of the Swarm satellite mission, for which the automatic TEC retrieval is intended, the created program is ready for application after the routines have been fit to the Swarm data formats and properties. Although the Swarm satellites are very similar to the CHAMP satellite, there are significant differences in the instrumentation concerning a TEC retrieval. Swarm employs a very sophisticated GPS receiver engineered by RUAG Austrian Aerospace which is especially designed for precise orbit determination. However, this GPS POD receiver can only track up to 8 satellites, which results in a lower data amount in comparison to the TRSR-2 receiver. As mentioned before, there will be no occultation devices since the GPS receiver only employs a POD antenna. This antenna is a so-called Patch Excited Cup (PEC) antenna that does not rely on choke rings to reduce multipath effects. The manufacturer declares the multipath error to be below 0.25 metres (RUAG Holding, 2010), which would improve the accuracy of the TEC determination results.

It is planned to integrate the TEC processing routines into the currently developed Swarm processor during an ESA supported project. This requires the creation of different test data sets covering typical properties of space-based GPS observations that are expected for the Swarm POD antenna. Since Swarm employs three satellites in different orbits, the implementation of the TEC processing has to be adapted to handle and distinguish between data with different properties. It is additionally aimed to extend the TEC processing to enable a combined analysis of the available data, which is preferable in order to benefit from the three-satellite-constellation. Analysing the data of three satellites simultaneously orbiting the Earth should not only increase the accuracy of the achievable TEC results, but also provide an improved insight in the temporal variations of TEC.

A. Configuration variables

Variable name	Value	Description
debug	1 or 0	additional information is printed to the screen during TEC processing
leo_rinex_dir	character string (max. 100 chars.)	Path of the LEO Rinex input files
leo_orbit_dir	character string (max. 100 chars.)	Path of the LEO orbit input files
gps_orbit_dir	character string (max. 100 chars.)	Path of the GPS orbit input files
gps_dcb_dir	character string (max. 100 chars.)	Path of the GPS DCB input files
input_by_year	1 or 0	Usage of additional year sub-directories for all input
tec_output	1 or 0	Results of the TEC processing are written out to a text file
tec_output_dir	character string (max. 100 chars)	Directory for the text output of the TEC processing
tec_plotting	1 or 0	TEC results are plotted or not
tec_plot_dir	character string (max. 100 chars)	Directory for the TEC plots
dcb_plotting	1 or 0	Receiver DCB results are plotted or not
dcb_plot_dir	character string (max. 100 chars)	Directory for the receiver DCB plots
multipath_plotting	1 or 0	Multipath results are plotted or not
multipath_plot_dir	character string (max. 100 chars)	Directory for the multipath plots
output_by_year	1 or 0	Usage of additional year sub-directories for all output
input_elevation_limit	0 - 90 (integer)	Elevation limit for data input
dcb_elevation_limit	0 - 90 (integer)	Elevation limit for initial receiver DCB estimation
dcb_sliding_avg	1 or 0	Calculation of sliding average during receiver DCB estimation
code_shift	"mean" or "median"	Method for code-to-carrier shifting
multipath_average_all	1 or 0	Multipath averaging over the whole time period of the TEC processing
path_delimiter	"/" or "\"	Character for delimiting all input and output paths
gnuplot_path	character string (max. 100 chars)	Path to the Gnuplot executable

Table 3: Configuration variables for TEC processing. For all variables with a switching function, 1 and 0 replace *true* and *false*.

B. Acronyms

AS	Anti-Spoofing
CHAMP	Challenging Minisatellite Payload
CHORB	CHAMP Orbit
DCB	Differential Code Bias
DLR	Deutsches Zentrum für Luft- und Raumfahrt (German Aerospace Center)
GFZ	GeoForschungsZentrum (German Research Centre for Geosciences)
GLONASS	Globalnaja Nawigazionnaja Sputnikowaja Sistema (Global Navigation Satellite System)
GNSS	Global Navigation Satellite System
GPS	Global Positioning System
IGS	International GNSS Service
ISDC	Information System and Data Center
JPL	Jet Propulsion Laboratory
LEO	Low Earth Orbit
NASA	National Aeronautics and Space Administration
NAVSTAR	Navigation System For Timing And Ranging
POD	Precise Orbit Determination
PPS	Precise Positioning Service
PRN	Pseudo Random Noise
RINEX	Receiver Independent Exchange
RMS	Root Mean Square
SA	Selected Availability
SPS	Standard Positioning Service
STAR	Space Triaxial Accelerometer for Research applications
TEC	Total Electron Content
TECU	Total Electron Content Unit
TRSR-2	Turbo Rogue Space Receiver-2
WGS	World Geodetic System

References

Anderson, D. and Fuller-Rowell, T. (1999). The Ionosphere.
http://www.swpc.noaa.gov/info/Iono.pdf, retrieved June 15, 2010.

Bauer, M. (2002). *Vermessung und Ortung mit Satelliten: GPS und andere satellitengestützte Navigationssysteme.* Herbert Wichmann Verlag, Berlin. 5. Auflage.

Blewitt, G. (1990). An automated editing algorithm for GPS data. *Geophysical Research Letters*, 17(3):199–202.

Bust, G. S. and Mitchell, C. N. (2008). History, current state, and future directions of ionospheric imaging. *Reviews of Geophysics*, 46.

Dana, P. H. (1998). GPS Satellite Signals.
http://www.colorado.edu/geography/gcraft/notes/gps/gif/signals.gif, retrieved June 24, 2010.

Foelsche, U. and Kirchengast, G. (2002). A simple "geometric" mapping function for the hydrostatic delay at radio frequencies and assessment of its performance. *Geophysical Research Letters*, 29(1473):4 PP.

Gurtner, W. (2007). RINEX: The Receiver Independent Exchange Format Version 2.10. ftp://igscb.jpl.nasa.gov/igscb/data/format/rinex210.txt, retrieved July 20, 2010.

Hartmann, G. K. and Leitinger, R. (1984). Range Errors due to Ionospheric and Tropospheric Effects for Signal Frequencies Above 100 MHz. *Bulletin Geodesique*, 58(2):109 – 136.

Heise, S. (2002). *Rekonstruktion dreidimensionaler Elektronendichteverteilungen basierend auf CHAMP-GPS-Messungen.* Freie Universität Berlin, Phd Thesis.

Heise, S., Stolle, C., Schlüter, S., Jakowski, N., and Reigber, C. (2003). Differential Code Bias of GPS Receivers in Low Earth Orbit: An Assessment for CHAMP and SAC-C.

König, R., Schwintzer, P., and Reigber, C. (2001). The CHAMP Orbit Format CHORB. http://op.gfz-potsdam.de/champ/docs_CHAMP/CH-GFZ-FD-002.pdf, retrieved July 20, 2010.

Lühr, H. (2010). The CHAMP Mission. Website of the CHAMP satellite mission: http://www-app2.gfz-potsdam.de/pb1/op/champ/index_CHAMP.html, retrieved June 16, 2010.

Montenbruck, O. and Kroes, R. (2003). In-flight performance analysis of the CHAMP BlackJack GPS Receiver. *in GPS Solutions, Springer-Verlag, Berlin*.

Prölss, G. W. (2004). *Physik des Erdnahen Weltraums: Eine Einführung*. Springer Verlag, Berlin. 2. Auflage.

RUAG Holding (2010). GPS Precise Orbit Determination. http://www.ruag.com/Space/Products/Digital_Electronics_for_Satellites_Launchers/ ↪Signal_Processing/GPS_Precise_Orbit_Determination_ , retrieved August 10, 2010.

Scherliess, L., Thompson, D. C., and Schunk, R. W. (2009). Ionospheric dynamics and drivers obtained from a physics based data assimilation model. *Radio Science*, 44.

Seeber, G. (2003). *Satellite Geodesy*. Walter de Gruyter, Berlin. 2nd edition.

Spofford, P. R. and Remondi, B. W. (1991). The National Geodetic Survey Standard GPS Format SP3. http://www.ngs.noaa.gov/orbits/sp3_docu.txt, retrieved July 20, 2010.

Stolle, C. (2004). *Three-dimensional imaging of ionospheric electron density fields using GPS observations at the ground and onboard the CHAMP satellite*. Phd Thesis. In: Wissenschaftliche Mittelungen aus dem Institut für Meteorologie der Universität Leipzig. Band 35.

Syndergaard, S. (2007). FORMOSAT-3/COSMIC ionospheric data processing and availability for data assimilation systems. Presentation at the IUGG XXIV General Assembly, Perugia, Italy, July 2 - 13, 2007 retrieved from http://www.cosmic.ucar.edu/groupAct/references/cosmic_iugg07.pdf, May 15 2010.

List of Figures

List of Tables

Affirmation in lieu of oath

Hereby I declare that I produced this master thesis independently and have not used outside sources and additives without declaration in the text. Any concepts or quotations taken from these sources are clearly indicated. This master thesis has not been submitted to other authorities of grading and has not been published elsewhere.

Neubrandenburg, September 1, 2010

Max Noja

Acknowledgements

This master thesis was supervised by Prof. Dr.-Ing. Andreas Wehrenpfennig. I would like to thank him for his scientific support, his critical examination of this work, and lots of hints, discussions, and suggestions in terms of software engineering. Special thanks is addressed to Dr. Claudia Stolle who proposed the subject of this thesis and acted as the secondary supervisor. I would like to thank her for numerous hints, suggestions, explanations, discussions, and her scientific support during this work.

Additionally, I want to thank Prof. Dr. Hermann Lühr, Dr. Stefan Heise, and Dr. Stig Syndergaard for their scientific support and for providing information and data which were necessary to create the program and results presented in this work.

A very big thanks goes to my parents who supported me in any way throughout my studies. For her support, motivations, and constructive distractions, I greatly thank my girlfriend Madlen.